Distribution Category:
Environmental Control Technology
and Earth Sciences (UC-11)

ANL-81-85
Part IV

ARGONNE NATIONAL LABORATORY
9700 South Cass Avenue
Argonne, Illinois 60439

RADIOLOGICAL AND ENVIRONMENTAL RESEARCH DIVISION ANNUAL REPORT

Atmospheric Physics
January—December 1981

A. F. Stehney, Acting Director
M. L. Wesely, Section Head

September 1982

Preceding Report

ANL-80-115 Part IV January—December 1980

The Atmospheric Physics Section investigates the physical behavior of the lower atmosphere and some of its chemical processes. A wide range of activities is reflected in this report, which emphasizes work for DOE but includes related work for other agencies also. As with previous annual reports, more thorough accounts of research by this Section can be found in the open scientific literature.

Acoustic sounding (SODAR) techniques are highly developed and have been applied to investigate a variety of phenomena in the planetary boundary layer, notably transport and dispersion over nonuniform terrain such as mountainous and coastal areas. One of the advantages of ground-based remote acoustic probing is that continuous averages of wind and thermal structure can be obtained more easily than with in situ techniques. These averages are desired, for example, to obtain better information on the thermally-driven mixing properties of the PBL and its relationship to surface exchanges of momentum, heat, and moisture. In these and related studies of transport, dispersion, and removal of pollutants in the boundary layer, work over simple uniform terrain continues in varying degrees, in order to provide a sound basis for extrapolation to more complex situations.

Research was concluded in 1981 on a DOE-sponsored analysis of wind characteristics in the lower 300 m of the atmosphere as measured on an Oklahoma City television tower. Some of the results from this short-term study are included in one article of this report. Work has continued on another DOE study, on the local behavior of pollutants emitted from diesel engines in urban areas. This year, effort was directed toward field studies on circulation patterns in steet canyons, exchange rates with the atmosphere above rooftops, and characterization of particles in outdoor urban microclimates. Substantial capability of measuring properties of atmospheric fine particles has been acquired to complement ongoing theoretical and wind-tunnel modeling efforts.

Surface layer meteorology remains a strong area of interest, especially as it concerns the exchange of trace materials between the surface and the atmosphere. Established micrometeorological methods have been applied in attempts to parameterize the air-sea exchange rates of carbon dioxide, in

research for DOE on the climatic effects of increased atmospheric carbon dioxide. Much of this and other boundary-layer research, and the associated development of experimental techniques, is strongly backed up by associated theoretical investigations.

A large share of the research is related to the "acid rain" issue, most widely discussed in connection with the acidification of lakes in the Northeast and Canada. Our participation is largely in support of EPA's Multistate Atmospheric Power Production Pollution Study (MAP3S). In addition to experimental work such as mentioned above on the transport, dispersion, and air-surface exchange of pollutants, there is considerable activity in numerical modeling. The Advanced Statistical Trajectory Regional Air Pollution (ASTRAP) model is heavily used for studying the long-range transport and deposition of sulfur and nitrogen compounds involved in acid rain. Other, more exploratory modeling deals with the detailed chemical and microphysical behavior of such contaminants in the atmosphere.

Also for MAP3S, considerable effort has been made to develop techn ues to study the chemical composition of precipitation and its re[illegible] .ships to atmospheric pollution and meteorological conditions, among [illegible] factors. The resulting data on local wet deposition have suggested some important mechanisms, have provided a sounder basis for interpretation of data from the National Atmospheric Deposition Program (NADP) wet deposition sampling network, and have yielded valuable information on precipitation chemistry in Illinois for use in research on effects on terrestrial ecosystems conducted by the Ecological Sciences Section of this Division.

Table of Contents

VERTICAL VELOCITIES DURING ASCOT 1980

R. L. Coulter

This section's participation in the Atmospheric Studies in COmplex Terrain (ASCOT) experiment in the Geysers area of California in September of 1980 included, in addition to Doppler sodar evaluations of horizontal winds (Coulter, 1981a, 1981b), investigation into vertical velocities over short time scales in order to study such things as thermals during daytime and vertical velocity distributions at night. During experimental periods, vertical velocities were averaged over a twenty-minute period; thus much of the small scale detail was not obtained. However, variances were calculated within each averaging period.

Vertical velocities (w) at the sodar site (see Fig. 1 of Coulter, 1981a) were predominantly positive (upward), both during day- and nighttime. Valley-to-mountain circulations dominated the daytime; overall mean vertical velocities are necessarily positive as the air rises with the slope of the valley. Superimposed upon this is the buoyancy dominated circulation of thermal plumes. During nighttime, average vertical velocities were often negligible, but on some nights there were well-defined positive values throughout the depth of the valley above the site. This may well have been due to convergence of the drainage flows from various directions into the outflow region. The vertical profile of w averaged throughout a nonexperimental night (Fig. 1) leads to a convergence value of about 0.0002 s^{-1}. This is a rather small value for what one might expect in the given terrain, but the sodar site was not located at the maximum convergency region. It should be noted that it was rare to observe a profile this smoothly well-defined during the experimental period. Profiles of w^2 are almost constant, and the w^3 profile shows a net transfer of energy upward in the lowest levels.

The variance profiles for the five experimental nights during September 1980 (Fig. 2) are similar to one another, with a constant or increasing variance with height to 250 m or more on all nights. There is, however, a difference of a factor of three in the overall magnitude through the five nights. Nighttime profiles taken in the relatively homogeneous

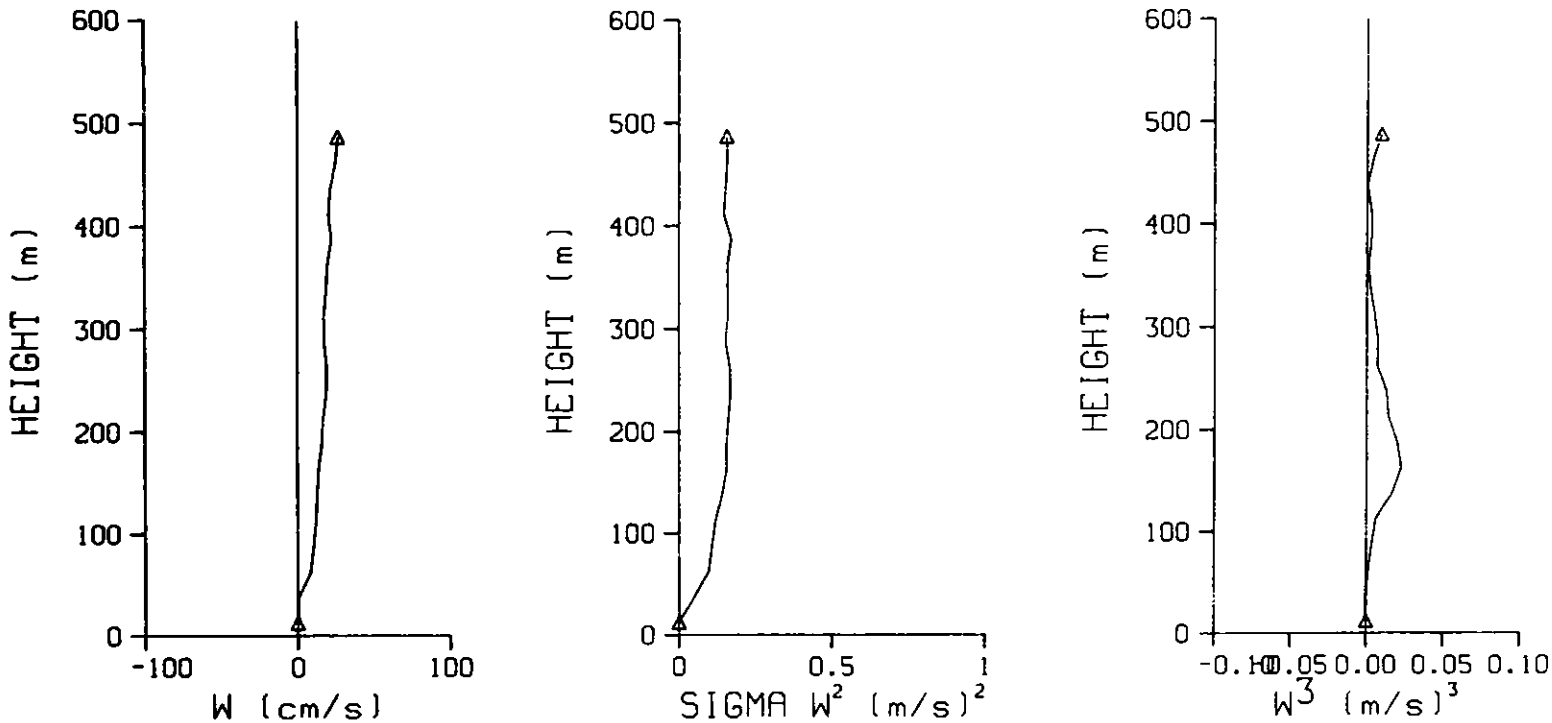

Fig. 1. Vertical velocity, variance and skewness for the night of August 20, 1980 in California.

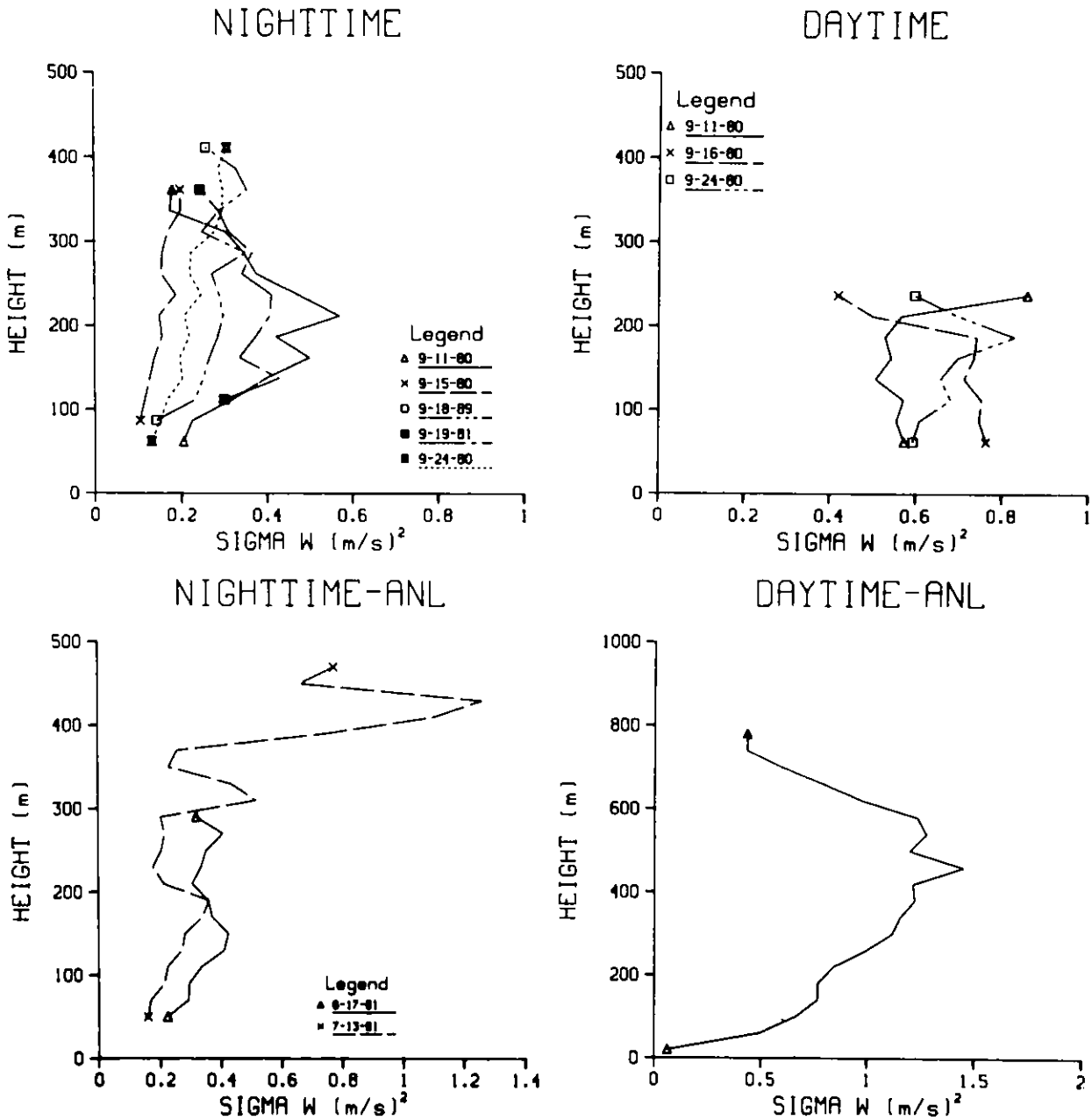

Fig. 2. Profiles of variance of vertical velocity for nighttime and daytime cases during ASCOT (top) and at ANL (bottom).

terrain at ANL also exhibit increasing values to near 150 m, which was roughly the inversion height on the nights shown, decreasing above that. (The large values above 300 m on July 13 correspond to an elevated inversion which descended during the night.) The magnitudes are also approximately the same as those from ASCOT. The larger depth for increasing variance in complex terrain probably originates from the mechanical mixing induced by terrain

features, which increases the depth of the nocturnal inversion and at times creates numerous elevated stratified layers within the valley.

Daytime variances during ASCOT on selected days illustrate a somewhat different character, in comparison with both nighttime (ASCOT) and daytime (ANL) values. The daytime values are larger than the nighttime values owing to the effect of buoyancy and separated, well defined plumes; however they are smaller by a factor of two or more than the flat-terrain daytime values at ANL during convective conditions with clear skies. In addition, the shape of the profile at ASCOT is relatively constant from about 50 m to above 200 m. In flat terrain, the profile normally increases with height to roughly one half the mixing height. Once again, terrain-induced mechanical mixing is offered as the probable cause. This turbulence causes the energy in the upper part of the flat terrain profile to be redistributed to lower levels, causing a more constant value of variance with height and a smaller average value through the profile. Values of the integrated variance from the two types of profile might be expected to agree, given the same value of surface heat flux. In the cases of Fig. 2, this is approximately true through 200 m. The ASCOT profiles in Fig. 2 were chosen to be as close in time as possible; other, deeper profiles exhibit the same behavior through 400 to 500 m.

Continued investigations into the 1980 ASCOT data may provide the spectral comparisons and necessary controlling factors (such as heat flux) to allow more exact comparison between profiles over complex terrain and those over homogeneous terrain.

References

Coulter, R. L., 1981a: Sodar investigations in Complex Terrain, Argonne National Laboratory, Radiological and Environmental Research Division Annual Report ANL-80-115, Part IV, pp. 1-4.

Coulter, R. L., 1981b: Circulation characteristics during ASCOT 1980, Preprint Volume, Second Conference on Mountain Meteorology, Nov. 9-12, 1981.

SODAR INVESTIGATION OF A LAKE BREEZE AT ANL

R. L. Coulter

Lake breeze circulations occur frequently around Lake Michigan during spring and summer. A lake breeze front is created by the cool, stable lake air pushing inland. In doing so, it collides with the air warmed by the land; the result is a turbulent interface between the two air masses similar to synoptic-scale fronts. The warm air forced over the denser lake air should rise at a mean rate determined by the speed and slope of the front. The turbulence generated by the mixing of the two air masses at the interface creates relatively large values of the temperature structure function C_T^2.

The ANL Doppler sodar was used to investigate the passage of a lake breeze front across Argonne on July 10, 1981. The lake breeze did not reach the Argonne site until after 1700 CST. Thus, the surface heating which drives the circulation had been substantially reduced, and the front was progressing mainly owing to momentum; subsequent development of an internal boundary layer due to surface heating could be expected to be diminished. The lake breeze front is clearly evident at 1720 CST, evincing an almost constant slope up to 800 m above the surface (Fig. 1). Assuming the frontal surface does not change shape and is moving at the mean wind speed behind it (3.7 m/s), the slope is roughly 0.4. After the frontal passage, there appears to be a small amount of surface based convective activity capped by an elevated inversion near 300 m. This may well be the height of the internal boundary layer which developed after the frontal passage, as a new mixed layer was reestablished beneath the overlying stable marine air. In this case, however, the frontal movement may have slowed enough (owing to the reduction of thermal forcing) that horizontal mixing of the internal boundary layer brought it close to the frontal surface itself. The near-surface convection observed after passage was probably due to instability created by the sudden influx of cooler marine air above the relatively warm surface, as there was no well-defined convective activity prior to the frontal passage.

A meteorological tower located approximately 100 m from the sodar recorded a surface temperature decrease of almost 1.5° C at 1715 CST and a wind shift at a 45 m height from 290° at 2 m/s to 90° at 3 m/s at 1718 CST.

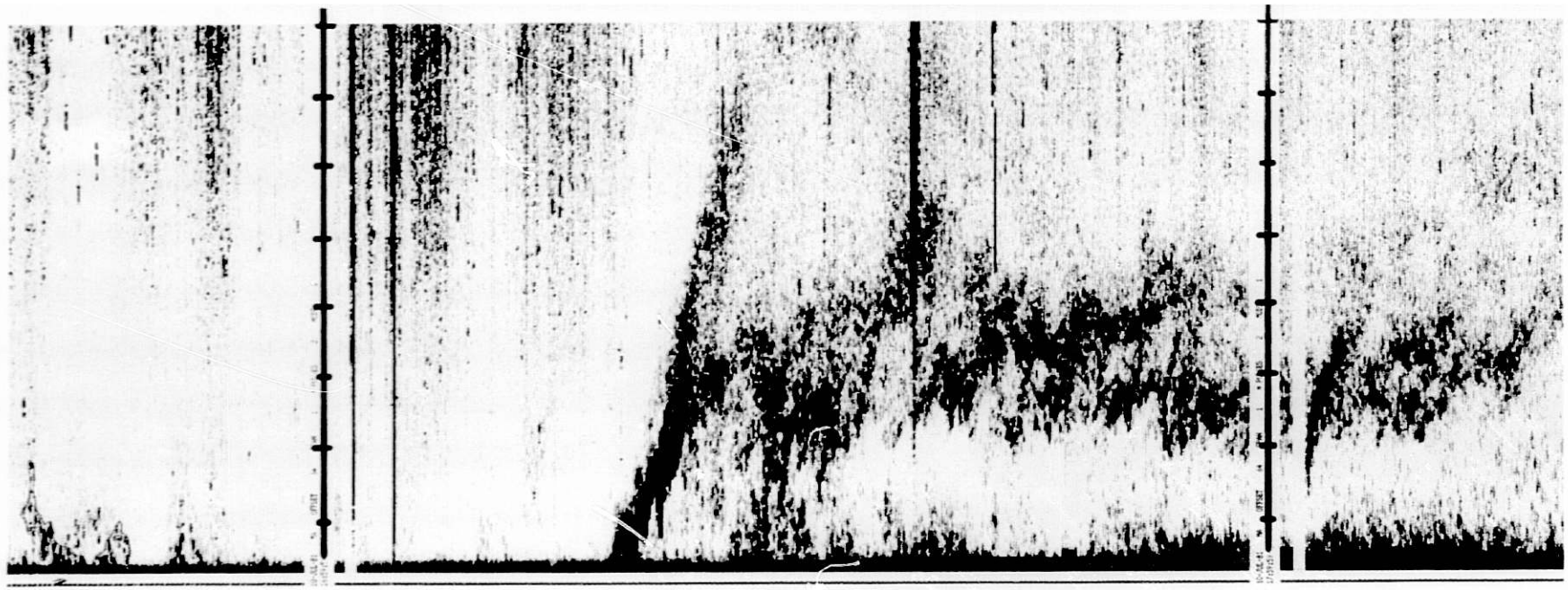

Fig. 1. Sodar record for period immediately before, during, and after lake breeze passage on July 10, 1981. Ordinate is the height above the ground in hundreds of meters; abcissa is time.

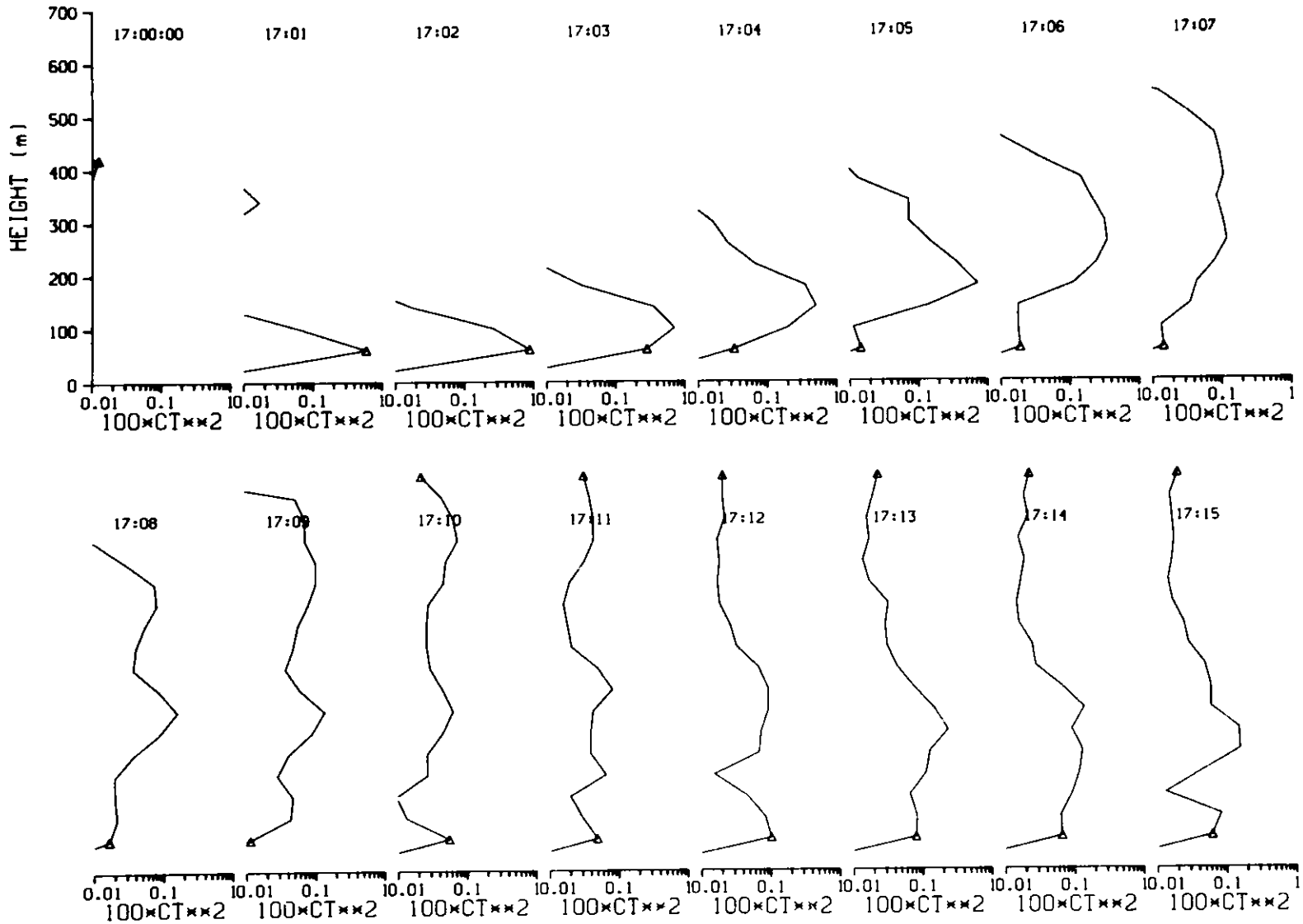

Fig. 2a. Sodar derived profiles averaged over 40 m at 1 min intervals during the frontal passage: C_T^2 values (0.0004 ~ 250 mV) less than 0.0001 are not plotted.

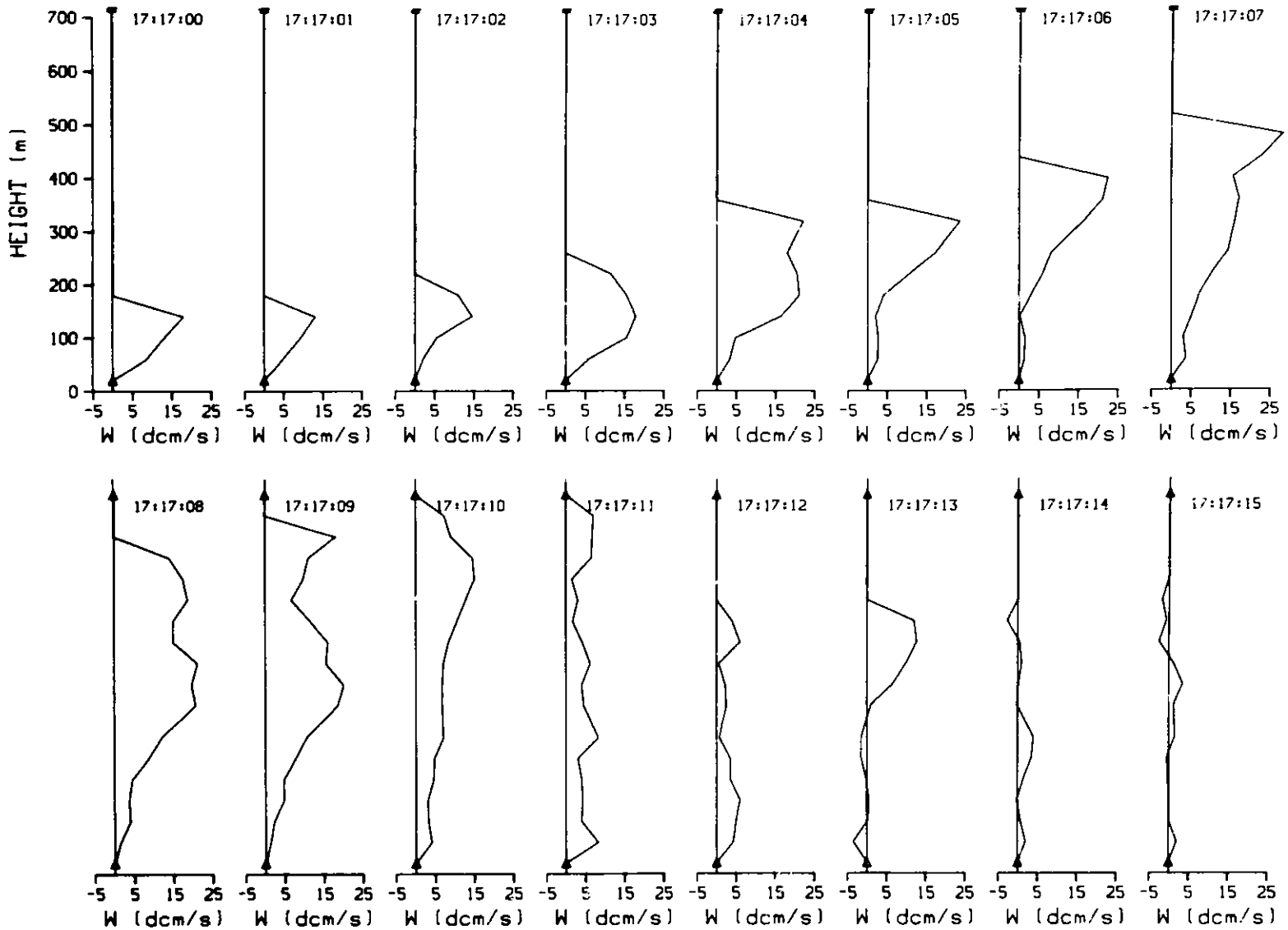

Fig. 2b. Sodar derived profiles averaged over 40 m at 1 min intervals during the frontal passage: Vertical velocity, decimeters/sec.

This temperature change is relatively small compared with that for other lake breeze passages observed at Argonne; however, the air temperature continued to drop in a linear fashion until 1900 CST, by which time the total decrease was 5° C. The wind direction returned to the southwest near midnight.

Figure 2 displays profiles of the vertical wind speed and C_T^2, at one minute intervals during and immediately after the frontal passage. Values of C_T^2 increase by nearly two orders of magnitude within the front itself up through 300 m. As the front passes by and the cool layer deepens, the increase over preexisting conditions is closer to one order of magnitude. Perhaps not coincidentally, the height of the elevated inversion behind the front is also at 300 m. Immediately following the frontal passage (1710), the C_T^2 profile to 300 m is roughly constant or log-linearly increasing. This indicates that the air behind the front had few characteristics of an unstable internal boundary layer, rather those of a stable internal boundary layer. Vertical velocities increase to nearly 2 m s^{-1} as the front reaches each altitude above the receiver. This corresponds reasonably well to the value of 1.6 m s^{-1} calculated from the rate of frontal passage over the site. It appears that there are positive velocities in the lowest 400 m for nearly 6 or 7 minutes after the frontal passage at those heights. After that time, values return to near zero throughout the profile.

Continuing studies of lake breeze frontal passages and characteristics are needed on a more consistent basis and with regional coverage in order to describe better lake breeze morphology and controlling factors on both large and small scales.

THERMAL PLUMES IN THE CONVECTIVE BOUNDARY LAYER

R. L. Coulter and C. Thoma

The daytime structure of the lower troposphere is often dominated by thermal plumes, those turbulent, yet ordered columns of relatively warm air rising into the mixed layer; in so doing, they distribute pollutants within the mixed layer. Because of their turbulent nature and relatively shallow penetration into the well-developed convective planetary boundary layer (PBL), thermal plumes lend themselves admirably to study by Doppler sodar. The strength of the temperature fluctuations is directly related to the amplitude of the returned signal, and the rise rate of the buoyant air can be detected via the Doppler shift of those same signals.

On several ideal cloudless occasions during 1981, the Doppler sodar was operated in a vertical mode to determine vertical velocities and amplitudes in an effort to investigate the nature of thermal plumes. There are two potential "signatures" of the plumes: the regions of strong reflectivity, which appear as dark, grasslike structure on a facsimile recorder, and the regions of well-defined positive vertical velocity.

In general, the plumes defined by strong reflectivity have relatively broad bases and become narrow with height. The maximum height of these plumes is about one-half the height of the well-mixed layer.

Part of the problem of relating either type of signature to a single characteristic thermal plume is that the sodar is an Eulerian sensor; as such it will see plumes only as they drift over the detector, observing but one vertical slice of each plume. In addition, the plumes themselves are in varying stages of growth or decay and may change in character as they pass. Thus, the variability from one plume to the next can be extreme, and a large sample is necessary to generate reliable statistics.

Rather than investigate individual plumes, one might examine the overall characteristics of the convective portion of the PBL, e.g., compare the turbulent fractions at different levels. This definition of thermals by sodar amplitudes (Fig. 1) leads to typical plume width (length of time with amplitude greater than a threshold value) decreasing roughly linearly with

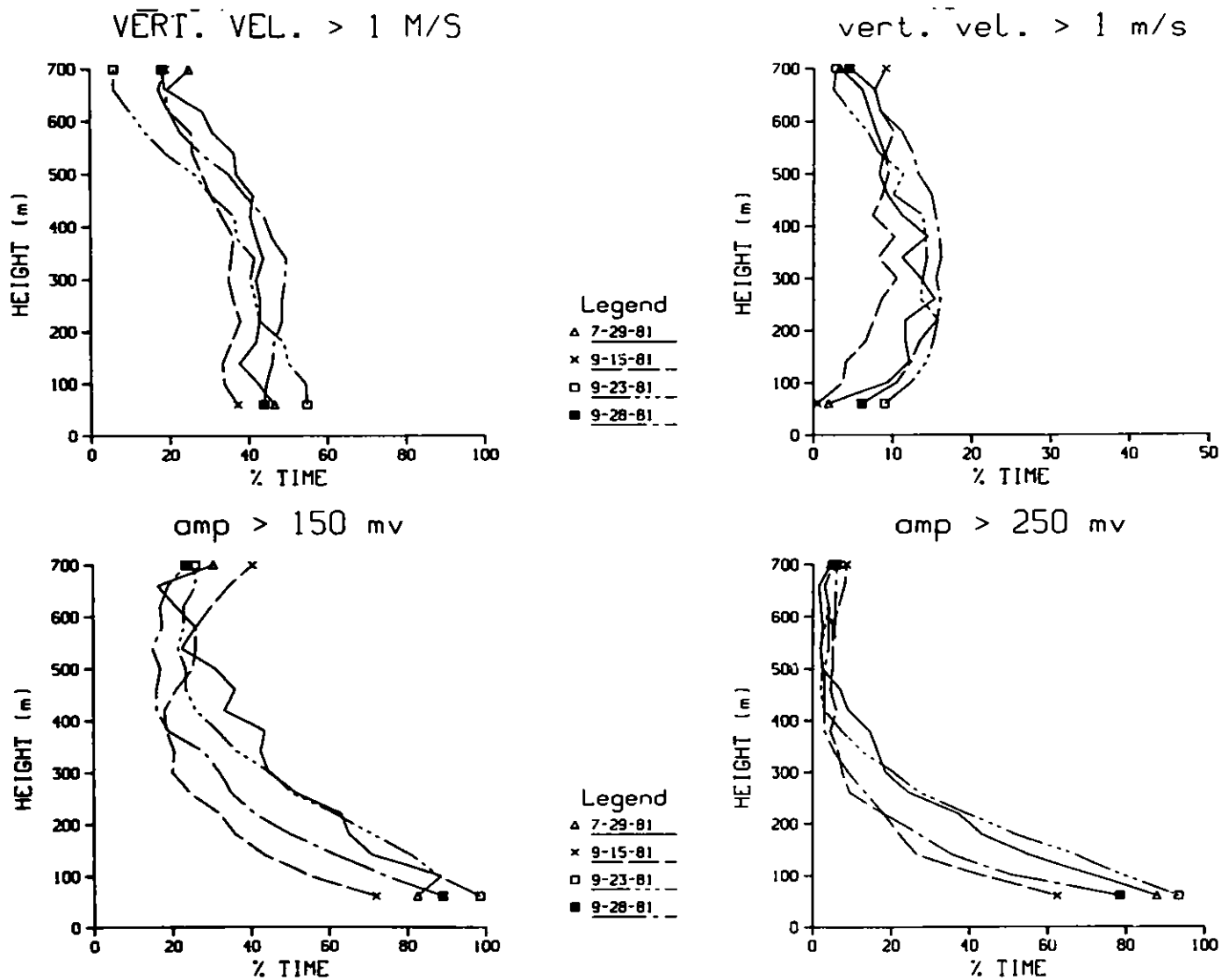

Fig. 1. Average characteristics of thermal plumes on four days in 1981. Four different threshold values for existence of plumes are used; an amplitude of 150 mV corresponds roughly to $C_T^2 \sim 0.00015$, 250 mV corresponds to $C_T^2 \sim 0.0004$.

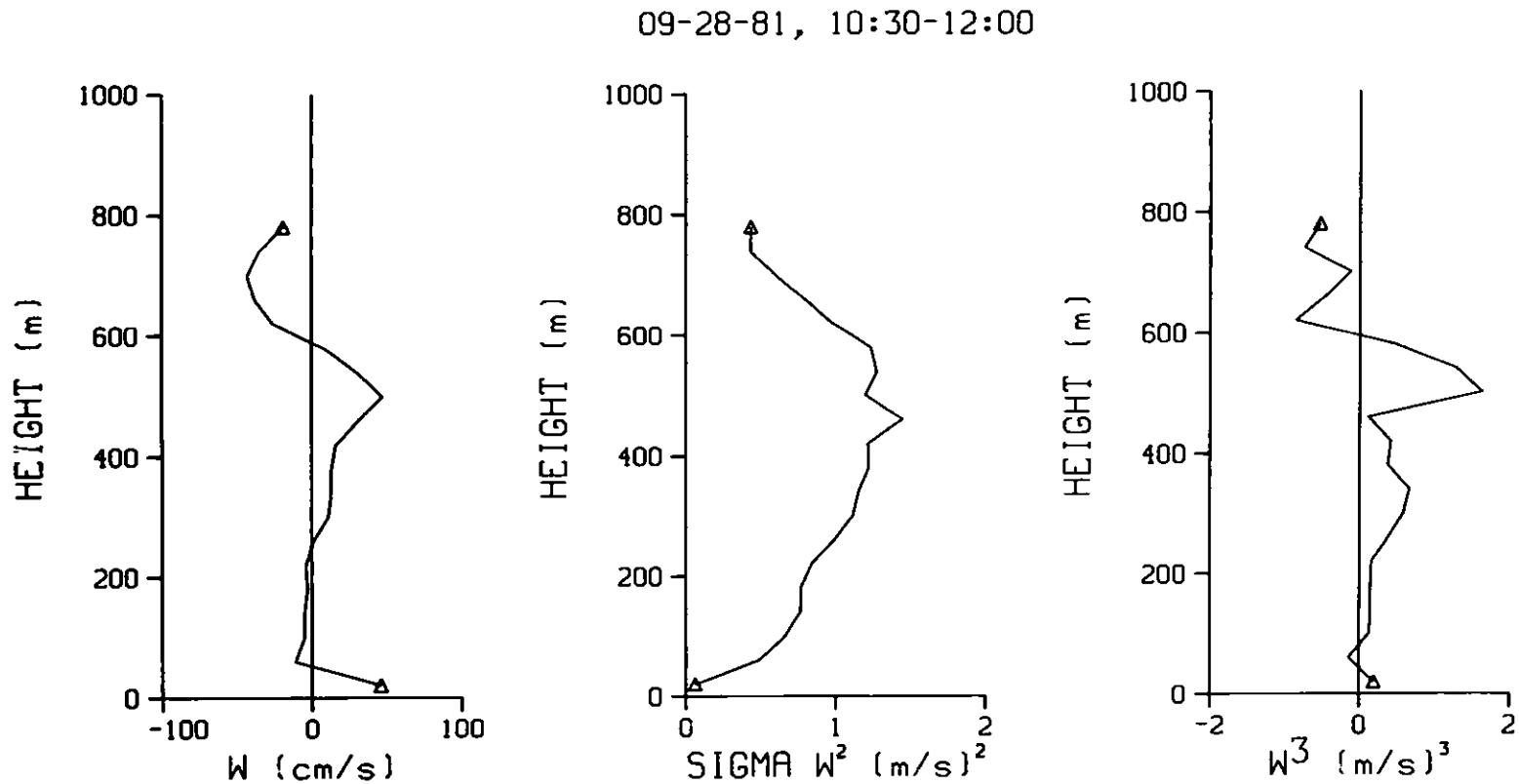

Fig. 2. Example of vertical velocity statistics for a short time on one of the experimental days.

height through the first 200 m. When the threshold is increased, that is, if only strong turbulent regions are included, the decrease remains linear to the same heights, but is greater. The velocity field, on the other hand, exhibits different characteristics. If one considers the threshold to be any positive vertical velocity, the plumes appear to have little narrowing with height through 300 to 400 m. If, however, the threshold is increased to 1 m s^{-1} (a large value) the widths increase with height to a maximum near 300 to 400 m, decreasing above. This implies that the largest positive velocities occur near 300-400 m as well. The picture which emerges is one in which the source region and the initial accelerations occur near the surface, where thermal turbulence and forcing are strong. The strength of the thermal turbulence decreases with height, but accelerations still take place. Thus, maximum plume velocities are achieved at a level where the thermal turbulence has decreased or stopped. The larger velocities lead to greater entrainment and the horizontal temperature gradient is reduced, but the region of rising air is broadened.

The profile of vertical velocity statistics during a typical day with a mixing height near 1000 m (Fig. 2) exhibits a well-defined peak in the variance profile near 500 m, as intense mixing is usually limited to the bottom half of the PBL. Note the transition to negative velocities above 600 m as turbulent parcels of air are mixed downward from the capping inversion. The skewness profile supports the intuitive notion that in the lowest regions the distribution of vertical velocities has a secondary peak or shoulder on the positive side, which corresponds to those found within thermal plumes.

Continued study of convection through the year will permit examination of the annual variation in the character of thermal plumes. Studies on cloudy days may show the modification, if any, due to the release of latent heat at the top of the mixed layer.

DISSIPATION RATE ESTIMATES FROM CIRCE

R. L. Coulter

As part of the Central Illinois Rainfall Convection Experiment (CIRCE), the Section Doppler sodar, under development at that time, was used to investigate vertical velocities and monostatic and bistatic amplitudes during both day and night. This provided the opportunity for an interesting experiment: the estimation of dissipation rates from independent sodar measurements of bistatic amplitude and vertical velocities. The data set available for this comparison is limited to three instances, all during daytime, when both bistatic amplitudes and monostatic vertical velocities were measured and recorded without pulse-to-pulse averaging.

Estimates of dissipation rate (ε) are quite straightforward, once the velocity structure parameter (C_V^2) is known, i.e.,

$$\varepsilon = (C_V^2)^{3/2}/2, \tag{1}$$

$$C_V^2 = \langle (w(z+\ell) - w(z))^2 \rangle / \ell^{2/3}, \tag{2}$$

where z is the height, ℓ is the distance between estimates of w, and $\langle\rangle$ indicates a time average. The velocity determination technique was that used by Gaynor (1977) and Melling (1980). Problems with this method are in two areas. The volume averaging of the sodar leads to underestimation of C_V^2, but Kristensen (1978) has derived a correction factor. A potentially more serious problem is due to the variance of vertical velocities implied in Eq. 2. The variance of vertical velocity determinations from sodar is a function of signal-to-noise ratios, frequency, number of samples used to determine w, receiver bandwidth, and range gate used, as well as atmospheric variations. The dependence upon system parameters was estimated by Spizzicino (1974) for spectral estimation techniques although others (Mastrantonio and Fiocco, 1981) have noted a field variance smaller than this theory predicts. The actual value of S, the variance associated with the data collection but not due to atmospheric variations, will be variable over short time scales and lead to instability in the estimate of C_V^2.

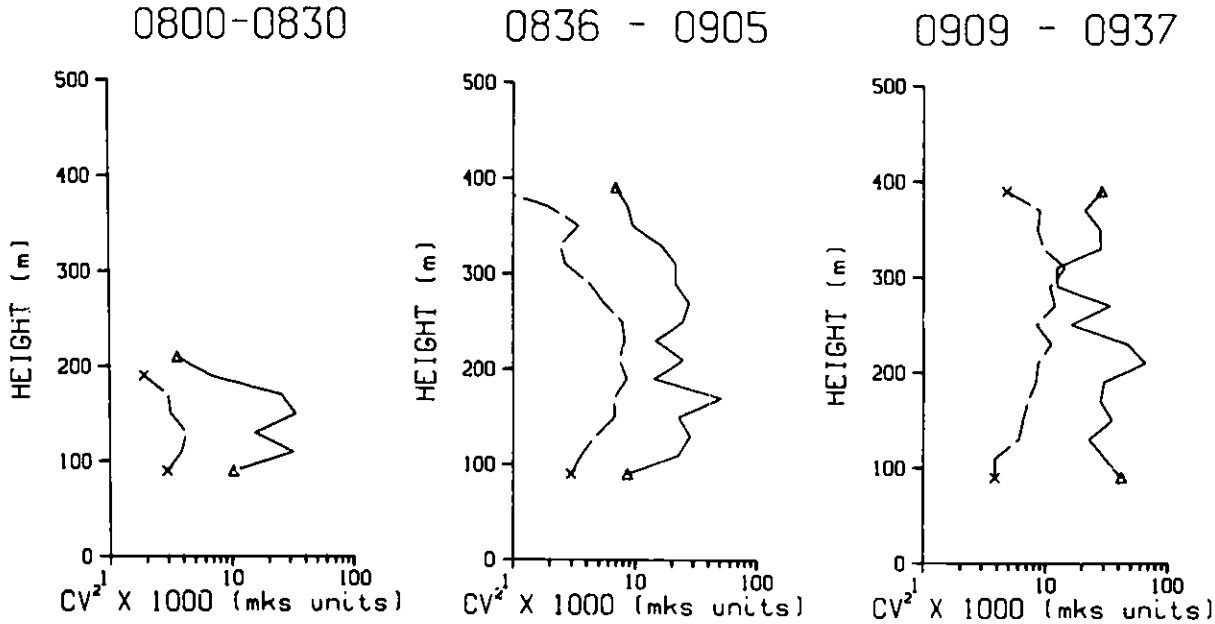

Fig. 1. Three consecutive profiles of C_v^2 from the morning of July 20, 1979. /--/ indicates determination from velocity differences; x--x, determination from bistatic sodar amplitudes. The difference in magnitude is a measure of S, the variance due to nonatmospheric variations.

Values for C_v^2 can also be obtained from sodar scattered amplitudes (Thomson and Coulter, 1974). These estimates are subject to errors due to antenna-beam weighting and the system function (Thomson et al., 1978; Kristensen, 1978) and the possible errors due to misalignment (Coulter, 1979). Nevertheless, this method has been used successfully (Thomson et al., 1978) for estimates of dissipation rates in both stable and unstable conditions.

Profiles of C_v^2 calculated both by velocity differencing techniques and by sodar amplitudes are shown in Fig. 1. In these estimates, individual velocity estimates were found by averaging data over several pulses, in order to reduce the value of S. The plots are not corrected for the effects of S because of the short time scale; however, a volume-averaging correction is included. Thus, the difference between estimates from velocity differencing and amplitude estimates can be viewed as a rough estimate of S. These data suggest a value of $S \sim 0.01\ m^2\ s^{-2}$. Both methods have the same profile characteristics, i.e., in the earliest profile the mixed layer is low (less than 200 m), and values of C_v^2 drop just above this height. As mixing

deepens, C_v^2 increases in magnitude and is approximately constant through the lower portion of the PBL.

These data indicate values of dissipation within the turbulent mixed region varying from, 0.00004 m^2 s^{-3} early in the morning to 0.001 m^2 s^{-3} one hour later when the mixed layer height had increased significantly. It appears, however, that use of the velocity differencing technique for dissipation rate estimation, particularly over short time scales, is difficult and dependent upon accurate knowledge of the variability in the velocity estimate due to system parameters.

References

Coulter, 1979: Sodar system function and error analysis, Radiological and Environmental Research Division Annual Report ANL-79-65, Part IV, pp. 30-34.

Gaynor, J. E., 1977: Acoustic Doppler measurement of atmospheric boundary layer velocity structure functions and energy dissipation rates, J. Appl. Meteorol. 16, 148-155.

Kristensen, L., 1978: On sodar techniques, Risø National Laboratory Report No. 381.

Mastrantonio, G. and G. Fiocco, 1981: Accuracy of wind velocity determinations with Doppler sodars, Internation Symposium on Acoustic Remote Sensing in the Atmosphere and Oceans, Calgary, Alberta, Canada.

Melling, H. and R. List 1980: Characteristics of vertical velocity fluctuations in a convective urban boundary layer. J. Appl. Meteorol. 19, 1184-1195.

Spizzichino, A. 1974: Discussion of the operating conditions of a Doppler sodar, J. Geophys. Res. 79, 5585-5591.

Thomson, D. W., and R. L. Coulter, 1974: Analysis and simulation of phase coherent acdar sounding measurements, J. Geophys. Res. 79, 5541-5549.

Thomson, D. W., R. L. Coulter, and Z. Warhaft, 1978: Simulation measurements of turbulence in the lower atmosphere using sodar and aircraft. J. Appl. Meteorol. 17, 723-734.

THE EFFECT OF SYSTEM GEOMETRY ON SODAR WIND SPEED ESTIMATES

R. L. Coulter

The Doppler sodar constructed at ANL has been used for gathering wind profile information in several studies (Coulter, 1980, 1981). An accurate determination of the wind speed at any given height must include effects of the beam patterns of transmitter and receiver, particularly at high wind speeds.

The usual procedure for defining the height (z) corresponding to the signal at any time is to assume the the acoustic energy travels directly from the transmitter to the position at height z directly above the receiver and thence directly to the receiver. In reality, however, the scattering volume covers an ellipsoid of revolution (Fig. 1), which includes the point at height z. Due to the antenna beam weighting, or directivity, the region near that point is most heavily weighted, and thus that point is often a good approximation. Moreover, as the transmitted pulse moves outward, the portion of the volume most heavily weighted shifts slightly relative to the point directly above the receiver.

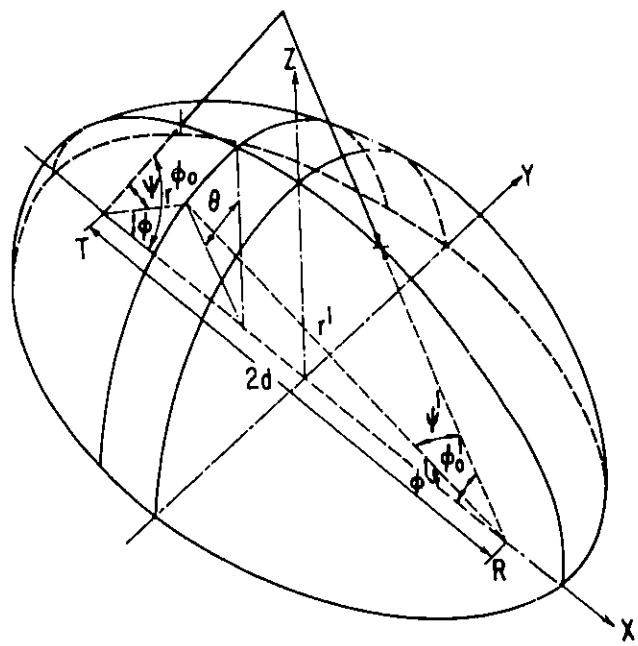

Fig. 1. Description of the coordinate system defined by bistatic system geometry. Usually the receiver pointing angle (ϕ'_o) is 90°, and height (z) is calculated directly above the receiver.

For heights less than those defined by the intersection of the receiver and transmitter axes, the scattering center will be shifted toward the transmitter because the strongest part of the transmitter directivity is to that side of the receiver. For heights larger than the intersection, the center will be shifted away from the transmitter. The calculation of the

exact amount of this shift (xbar) can be carried out using the directivities measured for the Argonne system (Coulter, 1978) and combining them with the scattering equation as in Kristensen (1978) to calculate the angular position of each scattering point, weighted by the directivities and the scattering cross section at that scattering angle, i.e.,

$$\text{xbar} = \int_0^{\pi}(x \cdot G(\gamma,\phi,a/d,F_t,F_r)d\phi / \int_0^{\pi}(G(\gamma,\phi,a/d,F_t,F_r))d\phi,$$

where G is as defined in Kristensen (1978), F_t and F_r are transmitter and receiver directivities, γ is the scattering angle, a is the semimajor axis of the ellipse, d is one-half the baseline, and ϕ is the elevation angle of the scattering point from the transmitter. Thus, the function G includes effects of both directivities and scattering cross section.

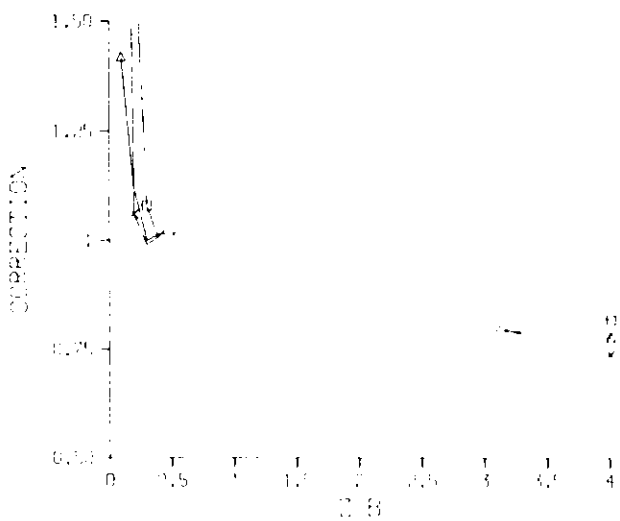

Fig. 2. Sodar correction factors derived from the directivity patterns of the ANL system for a frequency of 1300 Hz, at three different transmitter pointing angles: Δ = 45°; x = 50°; □ = 60°.

This weighted scattering position can be used to calculate the expected Doppler shift for a given horizontal wind speed, which can be compared to that calculated for a position directly above the receiver. Correction factors associated with the ANL Doppler system (Fig. 2) will change with frequency as the directivities change. Note that a constant factor has been added to the directivities for angles which deviate more than 20° from the pointing angle in order to simulate sidelobes at large angles and to

reduce computation time. The added factor has only slight influence, which occurs at large altitudes.

One can observe that there is a marked underestimate of wind speeds at small heights (quite often data at these heights are unused because of other difficulties, such as reflections from ground obstacles) and an overestimate at large heights. The dependence upon pointing angle of the transmitter is due to the change in intersection of the axes with the change in the pointing angle. The marked drop of the correction factor near $z/B = 0.3$ is created by the effect of the absence of scattering at angles of 90° . This offsets the shift toward the transmitter caused by the system functions as the scattering position approximately coincides with a scattering angle of 90°.

It is obvious that at large values of the height-to-baseline (B) ratio, the correction factor for a given system needs to be considered. Corrections near 20% can be expected for $z/B = 3$ (usually a maximum value for data gathering for this system), which can be near 4 m/s for very high wind speeds such as 20 m s^{-1}. At low wind speeds this correction is less important.

References

Coulter, R. L., 1978: Sodar calibration results, Radilogical and Environmental Research Division Annual Report, ANL-78-65, Part IV, pp. 14-18.

Coulter, R. L., 1980: Nocturnal low-level wind maxima at Argonne, Radiological and Environmental Research Division Annual Report, ANL-80-115, Part IV, pp. 8-11.

Coulter, R. L., 1981: Circulation characteristics during ASCOT 1980, Second Conference on Mountain Meteorology, Steamboat Springs, CO.

Kristensen, L., 1978: On sodar techniques, Risø National Laboratory Report No. 381.

EFFECTS OF SOIL MOISTURE ON EVAPOTRANSPIRATION FROM FESCUE GRASS

D. R. Cook

A simple model that parameterizes large-scale evapotranspiration in terms of surface type and near-surface (0-5 cm) soil moisture content is needed for applications of satellite imagery techniques. Such a model would also permit the estimation of large-scale sensible heat flux, a driving force for convective mixing of pollutants in the planetary boundary layer. The equilibrium model of Priestley and Taylor (1972), as modified by Davies and Allen (1973) gives

$$LE = \alpha'\left(\frac{S}{S + \gamma}\right)(R_n - G), \qquad (1)$$

where LE is actual evapotranspiration expressed as latent heat flux, S is the slope of the saturation vapor pressure-temperature curve, γ is the psychrometric coefficient, R_n is the net radiation, G is the surface soil heat flux density, and α' is the ratio of actual to equilibrium evapotranspiration. Equilibrium is defined to occur when the wet bulb depression at the surface is equal to that of the air.

Previous studies have shown that α' varies with surface type (plant species, height, stage of growth, root structure, etc.) and soil moisture, leading Barton (1979) to modify Eq. 1 to

$$LE = \frac{\alpha\sigma S}{\sigma S + \gamma}(R_n - G), \qquad (2)$$

where α is dependent on surface type and σ is a measure of surface moisture availability. Demonstration of the applicability of Eq. 2 to unsaturated vegetated surfaces has been limited by the dearth of evapotranspiration studies with measurements of near-surface soil moisture content. Besides the data of Davies and Allen (1973) and Williams et al. (1978), some measurements over an unsaturated surface were made by the author in 1975-1976. Previously analyzed for a different purpose, the data of Cook (1981) and Cook and Norman (1982) are reexamined here.

Seventy-one days of energy-budget and soil moisture measurements integrated over 24 hours were made over a small plot of tall fescue grass. Forty-three of the 71 days are not included in the following analysis because of interference from advection ($\alpha' > (S + \gamma)S^{-1}$), rain, or either freezing air temperatures or a frozen surface at some time during the day. Several other data points represent days when air saturation prevailed. As pointed out by Williams et al. (1978), evapotranspiration can occur under air saturation if sufficient temperature gradients exist to cause a vapor pressure difference between the surface and air. Although only seven days of G are available in the data set, the 24-hour integrated values are very small in comparison to R_n; therefore, following other investigators, calculations are performed without G. A first approximation to the lower limit of potential evapotranspiration is obtained from a linear regression line fitted to α' and LE/R_n; α' is equal to 1.25 at LE/R_n equal to 0.84, the latter being a lower limit suggested by Davies and Allen (1973) and Wilson and Rouse (1972) for a saturated surface (transpiration not limited by soil moisture content). Later analyses at a slightly lower limit of LE/R_n produce very similar estimates for α'.

An exponential expression for LE/R_n versus near-surface soil moisture content (M, in percent by volume) for the present data is

$$LE/R_n = 0.88(1 - \exp(-0.07M)), \qquad (3)$$

indicating that the field capacity soil moisture content M_f (the point at which the curve changes slope negligibly) occurs around M equal to 45. By another, independent regression analysis, it is found that coefficient α' can be expressed as a function of M_f as

$$\alpha' = 1.24(1 - \exp(-4.70M/M_f)), \qquad (4)$$

where the coefficient α' equal approximately to 1.24 has been assumed to be characteristic of the fescue grass for large values of M. Figure 1 shows the fit of Eq. 4 to the data.

Combining Eqs. 1 and 4, and assuming G to be negligible, we obtain

$$LE = 1.24 \frac{S}{S + \gamma}(R_n)[1 - \exp(-4.70M/M_f)], \qquad (5)$$

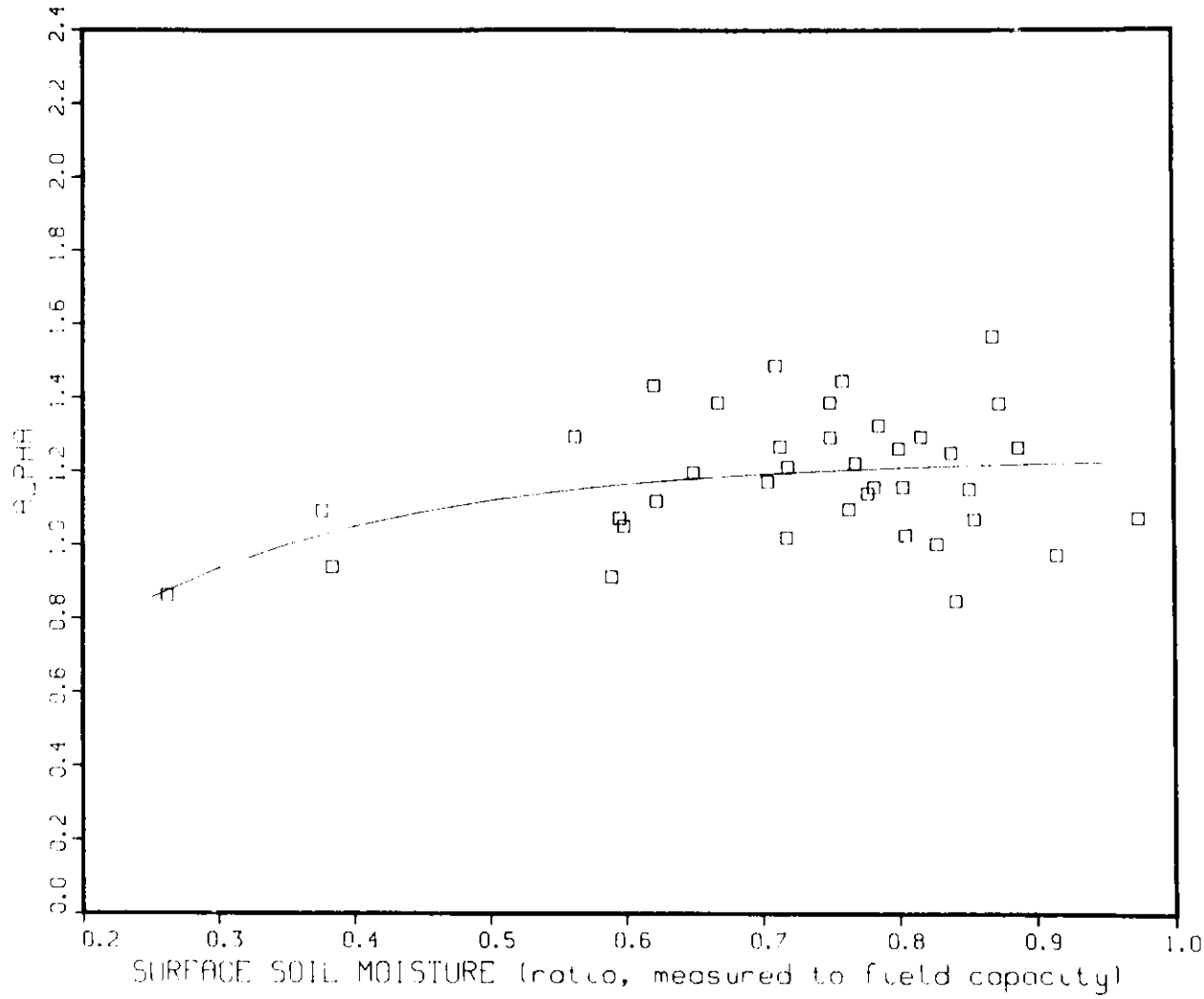

Fig. 1. α' versus near-surface (0-5 cm) soil moisture (M) content normalized by field capacity surface soil moisture (M_f).

which is similar to Eq. 3 in that both potential and nonpotential conditions can be described. It is less restrictive than Eq. 3 in that LE over soils with different values of M_f can be determined. However, the exponential forms of Eqs. 4 and 5 also include the effects of other soil properties and surface type, making the equations site-specific. To isolate the effect of varying soil properties from that of differring surface types, the procedure of Barton (1979) is followed; σ is determined from Eq. 2 for a value of α which is assumed (1.24 here) for a particular surface type. The curve drawn through the σ versus M data in Fig. 2 is well represented by the empirical expression

$$\sigma = 2.21M/(46.8 + M). \qquad (6)$$

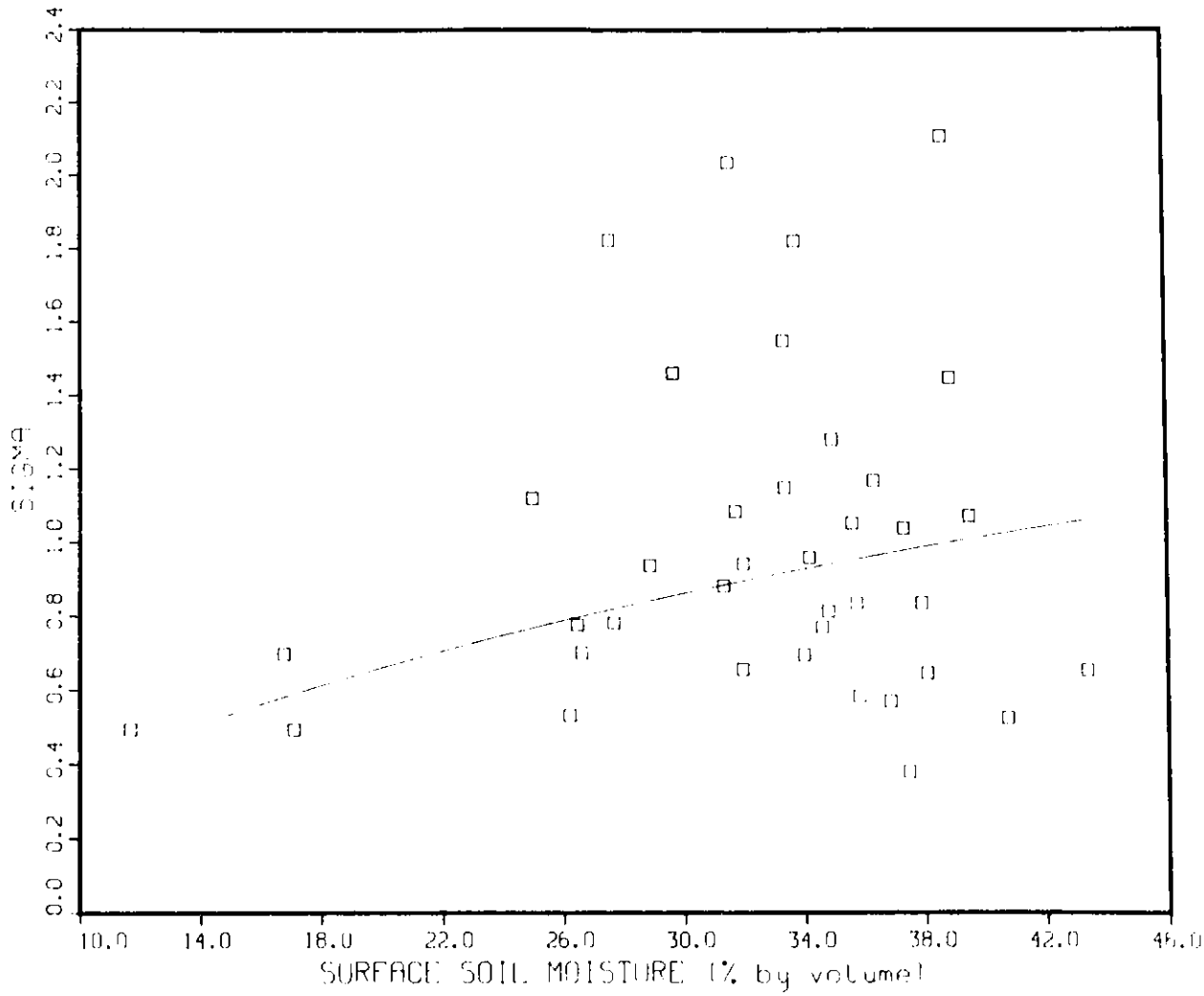

Fig. 2. σ versus near-surface (0-5 cm) soil moisture (M) in units of percent by volume.

For different soil conditions, different σ's can be employed. The equation produces σ equal to unity, an indication of surface saturation, when M is equal to 38.7. Thus, for this value of M and greater, potential evapotranspiration can occur. This implies that LE/Rn in Eq. 3 equal to 0.82 occurs at the lower limit of potential evapotranspiration.

Since all of the equations presented are a function of the temperature-dependent variables γ and S, the lower limit of potential evapotranspiration determined above is temperature-dependent as well. This effect was not investigated despite the large range of averge daily temperature (4.6 to 23.4°C, average of about 17.9°C) experienced during data collection. Indeed, this factor may have contributed to the scatter of the data in figures presented.

Equations 2 and 6 can be combined to produce an expression similar to Eqs. 3 and 5, but without an exponential term,

$$LE = 2.74MR_n/(2.21MS + 46.8\gamma + M\gamma). \qquad (7)$$

Since the soil and fescue grass root structure may differ for different sites, Eqs. 3, 5, and 7 are specific for one site. More important however, the results support previous findings of α' near 1.26 for grass surfaces. Since α and σ vary for different vegetation and soil types, it is necessary to conduct further studies over various surfaces. A study over field grass is planned for the summer of 1982 in the hope of adding to the knowledge of α', α and σ for grasses.

References

Barton, I. J., 1979: A parameterization of the evaporation from nonsaturated surfaces, J. Appl. Meteorol. 18, 43-47.

Cook, D. R., 1981: Waste heat utilization by soil warming, Argonne National Laboratory Radiological and Environmental Research Division Annual Report ANL-80-115, Part IV, pp. 82-85.

Cook, D. R., and J. M. Norman, 1982: Soil warming as an alternative to conventional waste-heat dissipation, J. Environ. Qual. 11, 46-52.

Davies, J. A., and C. D. Allen, 1973: Equilibrium, potential and actual evaporation from cropped surfaces in southern Ontario. J. Appl. Meteorol. 12, 649-657.

Priestley, C. H. B., and R. J. Taylor, 1972: On the assessment of surface heat flux and evaporation using large-scale parameters, Mon. Wea. Rev. 100, 81-92.

Williams, R. J., Broersma, K., and A. L. van Ryswyk, 1978: Equilibrium and actual evapotranspiration from a very dry vegetated surface. J. Appl. Meteorol. 17, 1827-1832.

Wilson, R. G., and W. R. Rouse, 1972: Moisture and temperature limits of the equilibrium evapotranspiration model, J. Appl. Meteorol. 11, 436-442.

A COMPARISON OF WIND SHEARS OF FRONTAL AND NON-FRONTAL SYNOPTIC CONDITIONS

C. M. Sheih

Wind shear considerations should play an important role in the design of large wind turbine generators. In the present study of wind shear, wind and temperature data gathered at seven levels 7, 26, 45, 89, 177, 266, and 444 m) on the 481-m WKY-TV tower, instrumented and maintained by the National Severe Storm Laboratory near Oklahoma City, Oklahoma, are classified into four categories: (I) disturbed (frontal passage), (II) undisturbed (non-frontal) conditions for all wind speeds, (III) undisturbed high wind speeds (greater than 6 m s^{-1}), and (IV) undisturbed low wind speeds (less than 6 m s^{-1}). The wind speed criterion is based upon measurements at the 26 m height, and the frontal passage periods are determined primarily from visual inspection of temperature records.

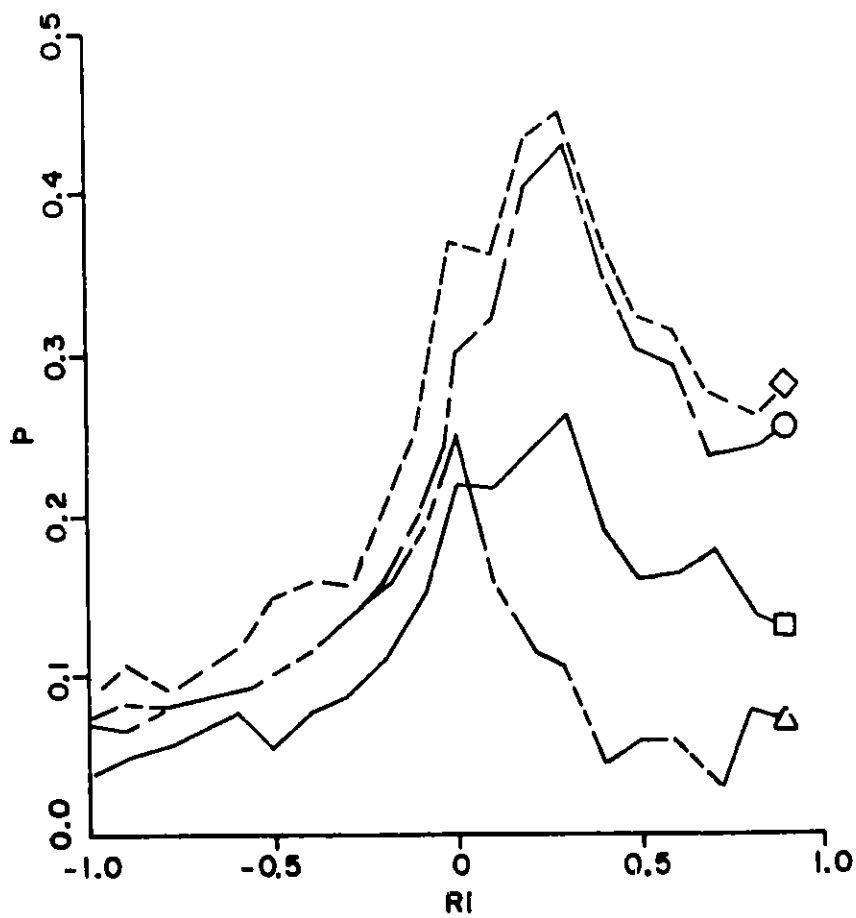

Fig. 1. The power law exponent p as a function of Richardson number in the lower atmospheric boundary layer for Categories (I) disturbed (□), (II) undisturbed, all wind speeds (○), (III) undisturbed, wind speed > 6 m s^{-1} (△), and (IV) undisturbed, wind speed < 6 m s^{-1} (◇).

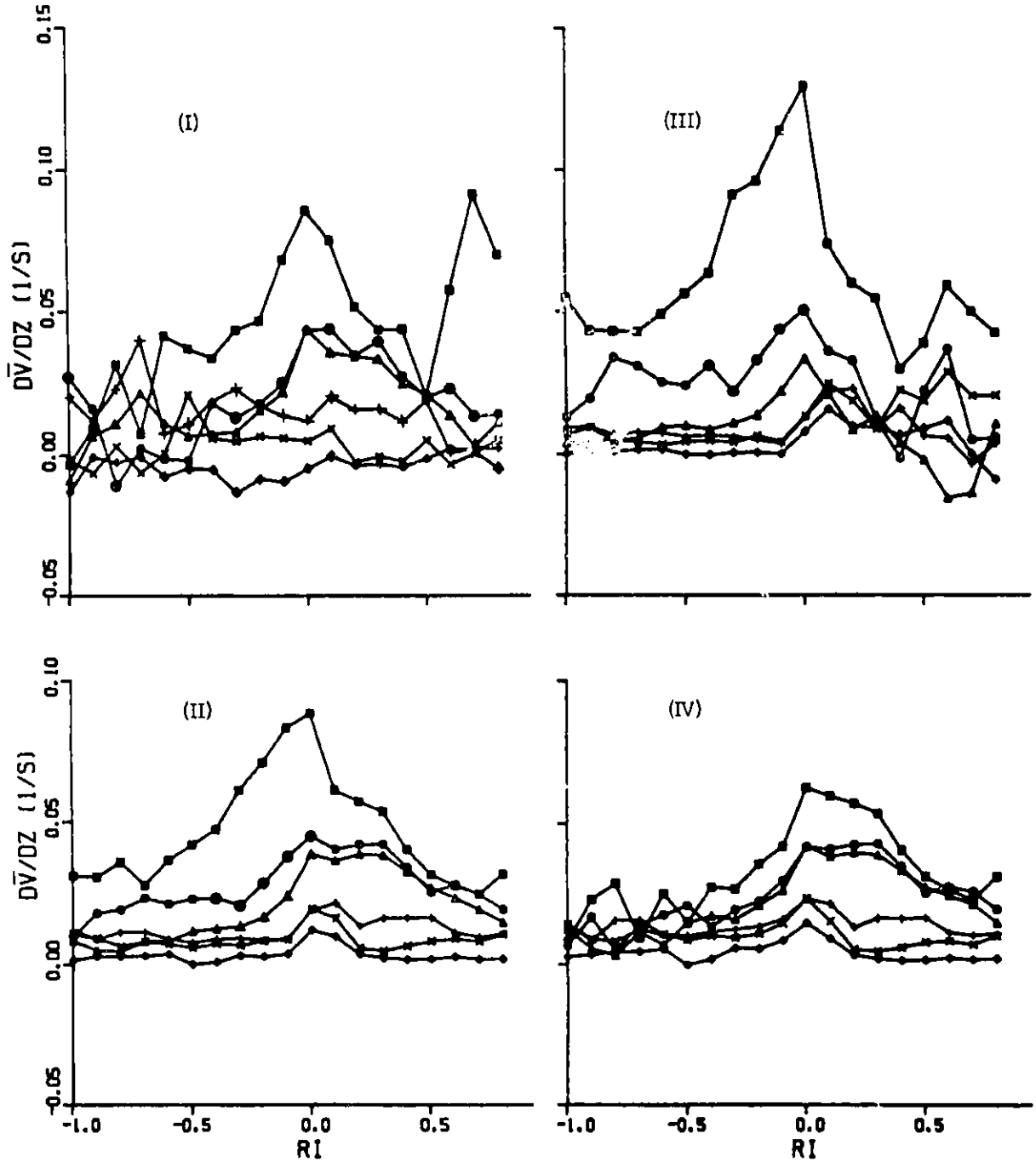

Fig. 2. Mean wind shear as function of Richardson number for various wind categories and heights, 7-26 (■), 26-45 (●), 45-89 (▲), 89-177 (+), 177-266 (×), and 266-444 m (◆).

To provide information for engineering applications, the exponential values (p) of the power law as a function of the Richardson number (based upon appropriate variables at 7 and 89 m) for the various wind categories are calculated. The results shown in Fig. 1 for Categories II and IV appear to be quite similar in both shape and magnitude to those reported by Heald and Mahrt (1981) for non-frontal wind conditions; but the values for categories I and III are much smaller than theirs, particularly for the stable side. Except for undisturbed high winds (III), exponential values peak around the "critical" Richardson number, 0.25. When the atmosphere is very unstable, the boundary layer is well mixed, resulting in small vertical wind velocity gradients and thus small values of p. As the atmospheric stability increases, turbulence intensity decreases and becomes less effective in transferring momentum to lower levels; consequently, the vertical velocity gradient and p increase. As stability increases beyond the critical Richardson number, the depth of the decoupled layer is reduced. However, it is not clear why the peak value for the high winds occurs at neutral atmospheric stability.

Mean wind shear as a function of height and Richardson number for each category is plotted in Fig. 2. The major differences between the frontal passages and undisturbed winds are that frontal passages have larger low-level mean wind shear at large positive Richardson values; the same features appear to a lesser degree in the high wind subset of undisturbed winds. Another difference is that frontal passages have a slight negative wind shear between the 266 and 444 m layer for $0.5 < Ri < 0.7$. Shear values for the undisturbed high wind cases are about twice those of the low wind case. Wind shears for all categories peak at neutral stability, and height and stability dependencies occur mainly below 89 m.

The corresponding standard deviations of wind shear fluctuations for each of the categories are shown in Fig. 3. There is no pronounced dependency on the Richardson number for frontal passages. However, for the undisturbed, all wind case, standard deviations are larger on the unstable side and smaller on the stable side for heights below 45 m, due to thermal production of turbulence. This trend is also seen in the high and low wind subsets. The outstanding wind shear feature of frontal passages seems to be the greater standard deviation of wind shear fluctuations on the stable side.

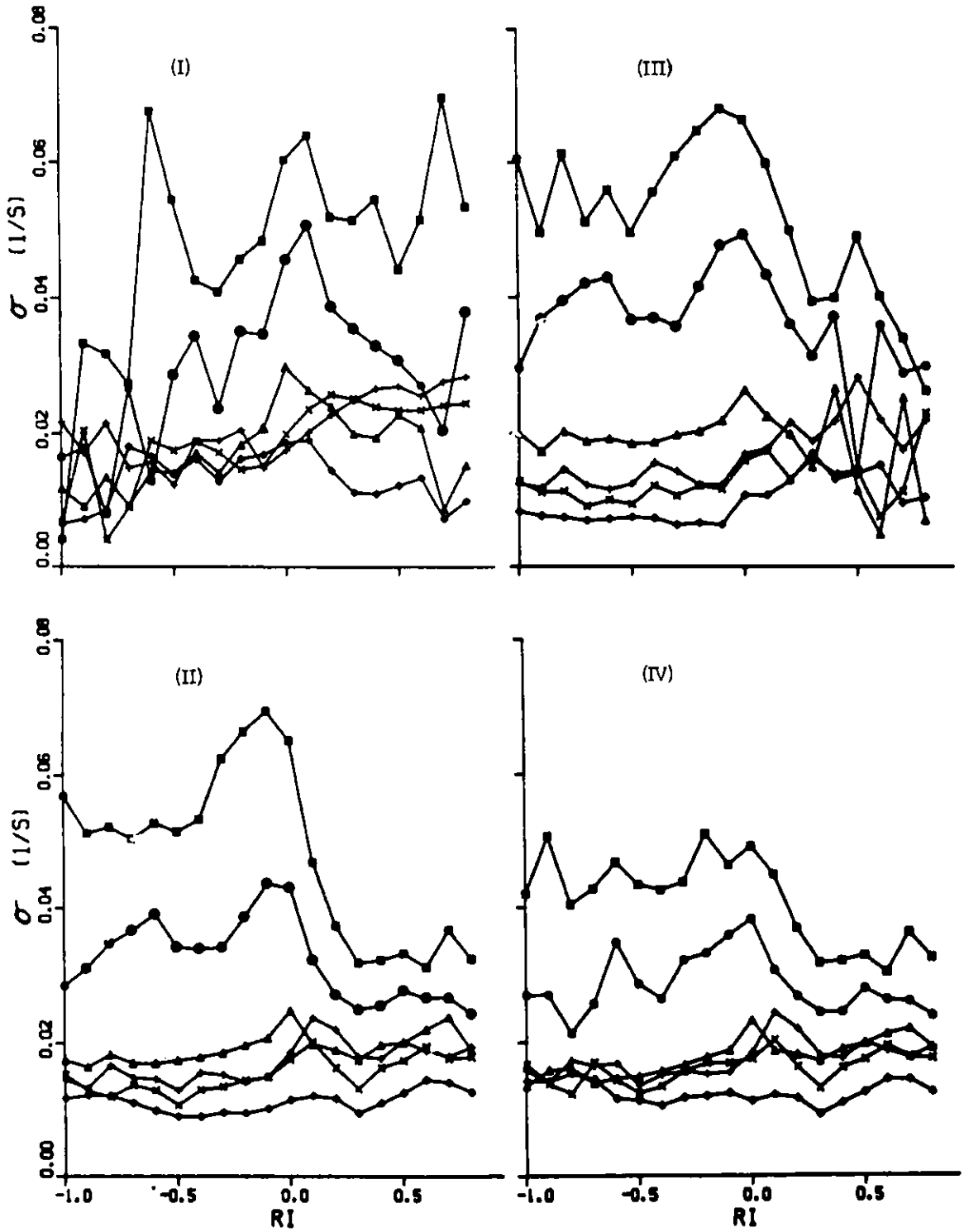

Fig. 3. Standard deviations of wind shear fluctuations as function of Richardson number for various wind categories and heights as indicated in Fig. 2.

Reference

Heald, R. C. and L. Mahrt, 1981: The dependence of boundary-layer shear on diurnal variation of stability. J. Appl. Meteorol. 20, 859-867.

MEASUREMENTS OF MEAN WIND VELOCITY IN A STREET CANYON WITH TRACER BALLOONS

C. M. Sheih, F. T. DePaul, and B. B. Billman

Dispersion in urban areas can be complicated by pollutants trapped in street canyons (e.g., Johnson et al., 1971). Knowledge of the wind velocity field within the canyon is essential in studying the problem; previous investigations include numerical simulations of mean wind velocity in various analytically described street canyons (Hotchkiss and Harlow, 1973), and qualitative laboratory observations using a flow visualization technique (Wang et al. 1972). The present study extends these investigations to real-world situations by releasing and tracking tracers in street canyons and provides direction for future studies of dispersion in urban areas.

Small balloons were chosen as the tracer since it was felt that they would minimize interference with urban activity. To simplify the problem for a preliminary study, a site of roughly uniform building heights (34 m) on both sides of a street of width 25 m was selected. The experiment was conducted only when the mean winds above roof level were nearly perpendicular to the street. The balloons were inflated to approximately equal buoyancy. In each experiment, twelve balloons distributed uniformly across the street in the middle of the block were released within 4 seconds. Photographs of the balloons were taken at one-second intervals with two cameras, one at the street level and another on a nearby roof. Coordinate points of each balloon were identified in the successive photographs to form a trajectory for each balloon. An example of trajectories is shown in Fig. 1. The velocity of each balloon was calculated at each position by finite differencing. The velocities of all the balloons in each set of releases were interpolated to give balloon velocities in a gridded coordinate system. To reduce the error due to non-uniform buoyancy of the balloons, an ensemble average of the gridded balloon velocities for various sets of releases was computed; the average balloon buoyancy velocity was then removed by constaining the vertical velocity integrated horizontally from wall to wall to be zero.

Figure 2 shows a sample result of the wind velocity vectors within the street canyon. The flow pattern appears to be quite similar to the numerical simulations of Hotchkiss and Harlow (1973) and this physical

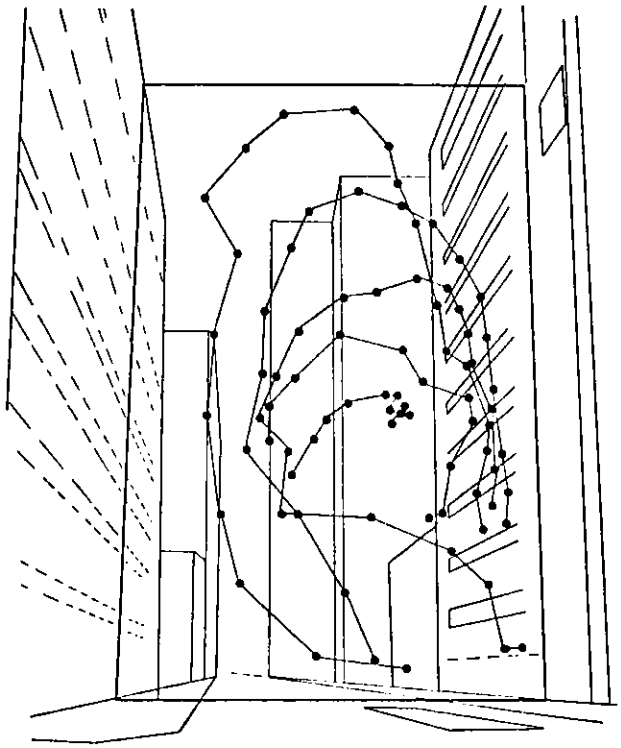

Fig. 1. Sample balloon trajectories in a street canyon.

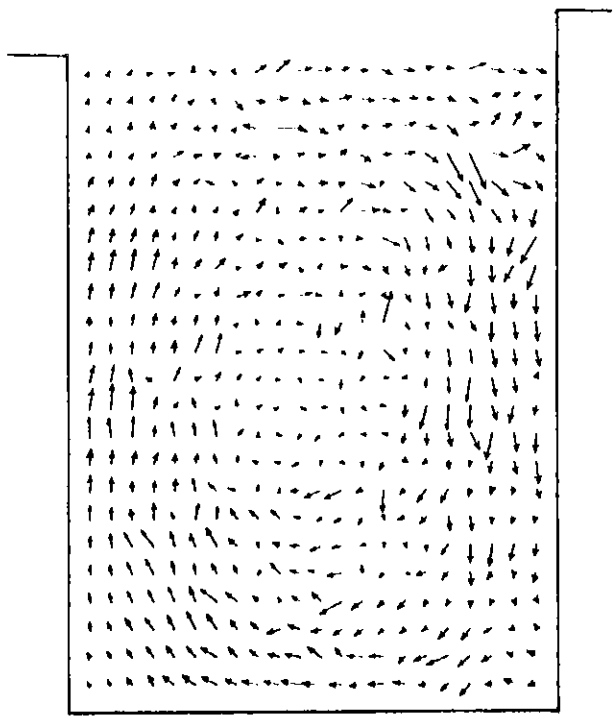

Fig. 2. Wind velocity vectors in a street canyon.

simulation of Wang et al. (1972), in which flow circulations are confined below roof level. However, it is quite different from flow circulations whose streamlines extend above the roof level, as assumed by Nicholson (1975) in formulating the distribution of pollutant concentrations in a street canyon. This suggests that the ventilation of emissions in a street canyon to the ambient upper air should be formulated with turbulent diffusion but not with a mean wind advection as made by Nicholson. A formula relating pollutant concentrations within the street canyon to those above roof level is under development.

References

Hotchkiss, R. S. and F. H. Harlow, 1973: Air pollution transport in street canyons, University of California, Los Alamos Scientific Laboratory, Los Alamos, New Mexico, Report No. EPA-R4-73-029.

Johnson, W. B., W. F. Dabberdt, F. L. Ludwig and R. J. Allen, 1971: Field study initial evaluation of an urban diffusion model for carbon monoxide, Comprehensive Report, Coordinating Research Council Contract CAPA-3-68(1-69), Stanford Research Institute, Menlo Park, California.

Nicholson, S. E., 1975: A pollution model for street-level air, Environ. 9, 19-31.

Wang, P. N., P. C. Chang, and A. Lin, 1972: Circulation and diffusion of the separation flow in a rectangular trough, University of Utah Scientific Report for the period 1 May 1970 to 30 April 1972, prepared for the Environmental Protection Agency under Grant AP-01126.

EXPERIMENTAL INVESTIGATIONS OF PRECIPITATION EFFECTS ON ATMOSPHERIC PARTICLE CONCENTRATION

F. T. DePaul and C. M. Sheih

Measurements of particle concentrations as a function of particle size were taken on two occasions during April 1981, as part of the Oxidation and Scavaging Characterization of April Rain (OSCAR) project, in order to characterize the aerosol size distribution before and after rainstorms; thus, the sampling events centered around a period of rain. The monitoring site was located adjacent to an open, short grass field approximately five miles southeast of Huntington, Indiana, well removed form the influence of local anthropogenic particle sources.

Particle size studied ranged from 0.0032 μm to approximately 10.0 μm. Particle sizes in the range of 0.0032 μm to 1.0 μm were monitored with a TSI model 3030 electrical aerosol analyzer, while particles of 0.3 μm to approximately 10.0 μm were counted with a Climet model 208A optical particle analyzer.

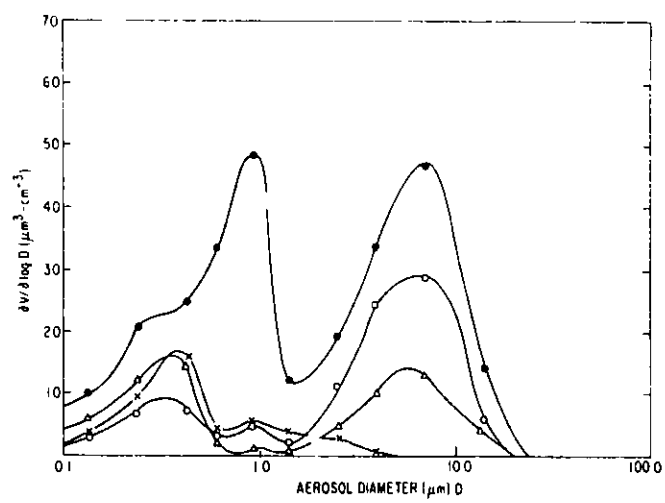

Fig. 1. Aerosol size distribution observed on April 8-9, 1981 for the hours of local standard times before the rain (●) 1600-2430, immediately following the rain (X) 0400 and (Δ) 0500, and after the rain (○) 0600-1700.

Figure 1 shows the size distribution of particles collected before, during, and after the rainstorm of April 9th. The pre-rain spectrum indicates a bimodal distribution, typical of background aged aerosols (Whitby, 1978). The distinct bimodal nature of the spectrum and the variation of volume concentration with time following rainfall for each mode indicate two independent methods of particle generation. The peak in the submicron

"accumulation mode" for the pre-rain samples is approximately 0.9 μm, substantially larger than typically found. This behavior may in part be explained by condensation of water vapor on particles under high humidity conditions as evidenced in the General Motors Sulfate Dispersion Experiment (Groblicki, 1976). During and after the rain the distribution of submicron particles appears to peak closer to the more nearly normal size (0.2 μm), and the amplitude remains relatively unchanged with time, whereas the supermicron particle distribution continuously experiences large changes during this period.

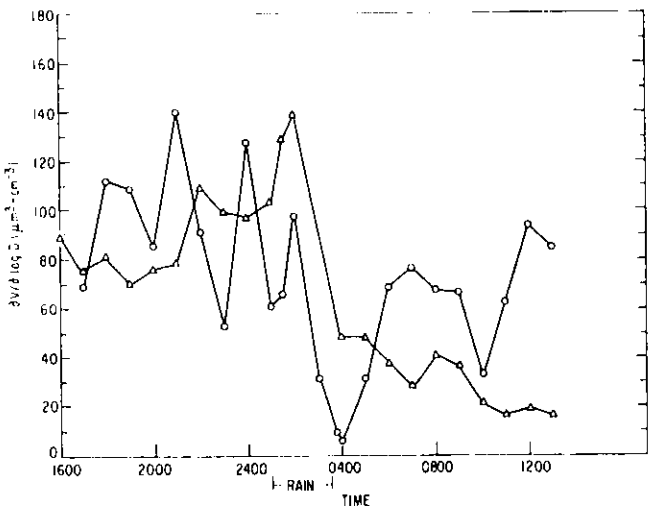

Fig. 2. Observed submicron (△) and supermicron (◯) concentrations for April 8-9, 1981.

The total volume concentrations for both submicron and supermicron modes (Fig. 2) show a rapid reduction in particle concentration during the rain. This reduction is probably due principally to the mechanisms of rainout, washout and advection of cleaner air. The "accumulation mode" continues to decrease as the cleaner, cold air mass moves through the area. However, pre-rain concentration levels of the supermicron particles are rapidly reestablished following the end of rainfall.

Estimates of scavenging rates based upon percent reduction in concentration between pre-rain and post-rain samples yield 22.8, 32.1, and 27.7% hr^{-1} for size ranges 0.1 to 1.5 μm, 1.5 to 10 μm, and 0.1 to 10.0 μm, respectively.

References

Whitby, K. T., 1978: The physical characteristics of sulfur aerosols, Atmos. Environ. 12, 135-159.

Groblicki, P. J., 1976: General Motors sulfate dispersion experiment: Aerosol sizing measurements, General Motors Research Publication GMR-2127.

MEASUREMENTS OF CO_2 TRANSFER VELOCITIES IN FRESH WATER AND OCEAN

M. L. Wesely, D. R. Cook, and R. L. Hart

Eddy-correlation measurements of the vertical flux density of CO_2 over water have been taken in a continuation of studies (Wesely et al., 1980) designed to parameterize the transfer velocity of CO_2 across the sublayer of water at the air-water interface. One experiment was performed over the fresh water of Lake Michigan with techniques and facilities used before (Williams et al., 1978; Wesely and Williams, 1980; Wesely et al., 1980), and one experiment was conducted with similar procedures over shallow coastal waters of the Atlantic Ocean near Miami, FL (Wesely et al., 1982). The results of these two experiments will be briefly described here.

Table 1 presents the data taken over Lake Michigan, where u_* is the friction velocity, z/L is the atmospheric stability parameter defined by the ratio of height of measurement (z = 8 m) to the Obukhov length L, v_t is the transfer velocity (positive upwards), and H is a Henry's Law constant. The product $v_t H^{-1}$ is the flux divided by the concentration difference across the uppermost skin of water, as referred to equilibrium concentrations in the atmosphere close to the surface. The values of $v_t H^{-1}$ display some variability, but average close to 0.0010 cm s^{-1} with a standard error of 0.0002 cm s^{-1}, and correspond to values of u_* equal to 8.6 ± 0.5 cm s^{-1}. The variability of measured $v_t H^{-1}$ is typical and indeed corresponds to a standard error near $0.0008/n^{1/2}$ as predicted earlier (Wesely et al., 1981).

The calculation of transfer velocity for the Lake Michigan experiment assumes that the partial pressure of CO_2 in the water was zero. This is partially justified because of the water's high pH (near 8.3), which apparently was associated with the typical algal bloom that occurs at times in Lake Michigan. The assumption of zero partial pressure of CO_2 indicates that the transfer velocities calculated are a lower bound and as such they roughly agree with predictions derived from radon-evasion studies (e.g., Peng et al., 1979).

Transfer velocities found at the oceanic site radically depart from the radon-evasion predictions. Data were taken from an unmanned lighthouse (Fig. 1) about 30 km from the mainland near Miami, FL, and above water 2 to

Table 1. Half-hourly averages of CO_2 transfer velocity $v_t H^{-1}$ and other quantities over Lake Michigan on July 7 and 8, 1981.

Time (CST, center)	u_*, cm s^{-1}	z/L	CO_2, ppm	$v_t H^{-1}$, cm s^{-1}
1415	7.0	0.23	344	0.0003
1445	6.9	0.26	348	-0.0001
1515	8.8	0.13	348	-0.0001
1545	10.2	0.14	339	0.0000
1615	11.6	0.19	335	0.0019
1645	11.9	0.22	340	-0.0021
1745	11.9	0.27	350	-0.0038
2315	7.3	0.77	373	-0.0014
2345	6.6	0.46	373	0.0001
0115	5.0	0.72	373	-0.0013
0145	6.5	0.82	373	-0.0012
0215	7.5	0.59	373	-0.0014
0245	6.7	0.54	373	-0.0005
0315	8.0	0.43	374	-0.0008
0515	6.1	1.00	372	-0.0027
0545	6.2	0.66	372	-0.0026
0615	7.4	0.25	372	-0.0009
0645	8.8	0.36	372	-0.0019
0715	12.6	0.33	372	0.0002
0745	14.4	0.27	372	-0.0024
0815	7.0	0.87	373	-0.0011
0845	9.0	0.47	374	-0.0005
0915	8.5	0.59	375	-0.0004
1015	3.2	1.00	375	-0.0011
1045	5.2	0.95	375	-0.0017

Fig. 1. The Fowey Rocks lighthouse from which the oceanic data were taken. Instruments were suspended from a boom pointed upwind of the lighthouse and the wooden pier at the lower right-hand portion of the photograph.

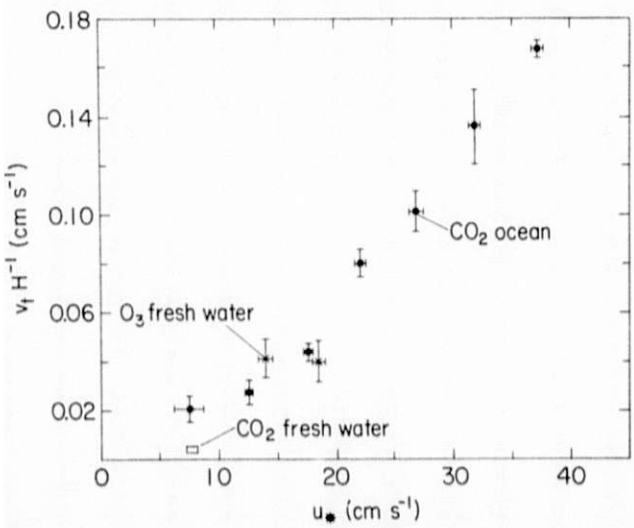

Fig. 2. Summary of transfer velocities measured for water surfaces. The error bars shown indicate standard deviations.

8 m deep. Figure 2 shows the results; the transfer velocities found are 20 to 60 times greater than those indicated by the radon-evasion data, with the greatest departures occurring at the higher wind speeds. During these experiments the gradient of CO_2 across the air-sea interface was found to be about 100 ppm. Shown for comparison are averages of the data from Table 1, and ozone data derived from Wesely et al. (1981), with both transfer velocities inverted in sign in order to use the graph in the present configuration. The mean ozone transfer velocity, which is multiplied by 3.4 to take into account the different values of Henry's Law constants, is large probably because of some chemical destruction of ozone at the water surface (Wesely et al., 1981).

This work indicates that CO_2 fluxes over ocean might be much larger than expected. The reasons for this remain largely unexplained; chemical reactions at the surface might play some role. Of course, there might be some sources of experimental error, but none has been found that would create such large deviations. It should be remembered that the oceanic results presented are specific to upward fluxes over shallow coastal waters where a rather large excess of CO_2 exists in the water. Measurements over open ocean are needed, so that the exchange of CO_2 between the air and ocean on a global scale can be calculated with the use of accurate parameterizations.

References

Peng, T.-H., W. S. Broecker, G. G. Mathieu, Y.-H. Li and A. E. Bainbridge, 1979: Radon evasion rates in the Atlantic and Pacific Oceans as determined during the GEOSECS Program, J. Geophys. Res. 84, 2471-2486.

Wesely, M. L. and R. M. Williams, 1980: Eddy-correlation measurements of particle fluxes over Lake Michigan, Argonne National Laboratory, Radiological and Environmental Research Division Annual Report ANL-80-115, Part IV, pp. 36-38.

Wesely, M. L., D. R. Cook and R. M. Williams, 1980: Preliminary measurement of CO_2 flux, Argonne National Laboratory, Radiological and Environmental Research Division Annual Report ANL-80-115 Part IV, pp. 39-42.

Wesely, M. L., D. R. Cook and R. M. Williams, 1981: Field measurement of small ozone fluxes to snow, wet bare soil, and lake water, Boundary-Layer Meteorol. 20, 459-471.

Wesely M. L., D. R. Cook, R. L. Hart, and R. M. Williams, 1982: Air-sea exchange of CO_2 and evidence for enhanced upward fluxes, J. Geophys. Res., in press.

Williams, R. M., M. L. Wesely and B. B. Hicks, 1978: Preliminary eddy-correlation measurements of momentum, heat and particle fluxes to Lake Michigan, Argonne National Laboratory, Radiological and Environmental Research Division Annual Report ANL-78-65, Part IV, pp. 82-87.

SOME PROPERTIES OF SCALAR TRANSPORT IN THE ATMOSPHERIC SURFACE LAYER

M. L. Wesely, R. L. Hart, and D. R. Cook

The turbulent behavior in the atmospheric surface layer of pollutant species, such as ozone, sulfur dioxide and submicron particles, is much less understood than the widely investigated behavior of temperature and water vapor. As a result, studies of pollutant vertical transfer or deposition from the atmosphere use assumptions derived from work on the latter (and to a less extent, on carbon dioxide). For example, the aerodynamic resistance to vertical transport of pollutants in the surface layer is assumed to be the same as or very near that computed for heat (Wesely and Hicks, 1977). A clear distinction is made between the properties of scalar quantities and those of momentum, a vector quantity or, more correctly, a representation of the surface stress tensor. The assumption of equal aerodynamic resistance is equivalent to saying that the eddy diffusivities are identical, a concept more commonly used in the scientific literature.

This report examines the relation between fluctuations of temperature T, ozone χ, and humidity q in the atmospheric surface layer over uniform short vegetation, a soybean field. The spectral properties of temperature fluctuations have been studied by numerous investigators, and it is known that T and q fluctuations are highly correlated over warm vegetation at frequencies associated with eddies that carry the scalar quantities vertically. This high degree of correlation supports the contention that the transfer characteristics of these two scalar quantities are similiar, if not that the eddy diffusivities are equal, because of the implication that eddies transport heat and water vapor in an identical fashion. Also, a high correlation between q and T fluctuations indicates that the normalized cospectra of T and of q with the vertical wind component w are nearly identical. This is quite useful in correcting eddy-correlation measurements of the vertical water vapor flux for inadequate frequency responses of the w and q sensors, because the w-q cospectral estimates needed for the corrections can then be readily inferred (e.g., Wesely et al., 1978). It will be shown that ozone fluctuations are highly correlated with T and q fluctuations. By inductive reasoning, this leads to some justification for assuming that the

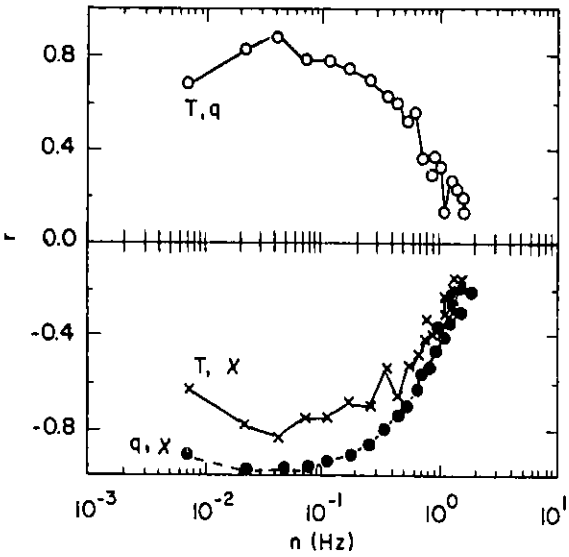

Fig. 1. Spectral correlation coefficients for a 25 min period during unstable conditions over soybeans. Mean wind speed was 280 cm s^{-1}, sensible heat flux 54 W m^{-2}, latent heat flux 390 W m^{-2}, and ozone deposition velocity 0.7 cm s^{-1} at a 5 m height.

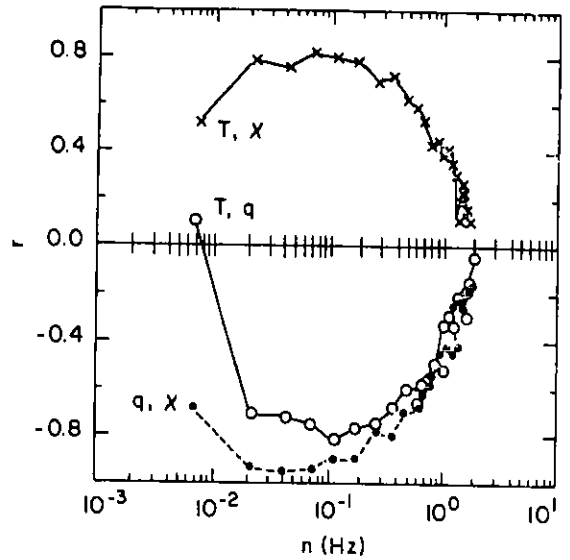

Fig. 2. Spectral correlation coefficients as in Fig. 1 except during stable conditions, a wind speed of 400 cm s^{-1}, sensible heat flux of -11 W m^{-2}, latent heat flux of 125 W m^{-2}, and ozone deposition velocity of 0.5 cm s^{-1}.

eddy diffusivities for many scalar quantities are identical and that corrections of eddy-correlation estimates for inadequate sensor responses can be made using the same procedures as used for heat-flux corrections.

Figures 1 and 2 show the spectral correlation coefficients, which are the cospectra divided by the square roots of the products of spectral values, between pairs of T, q and χ, measured in dry deposition studies conducted over soybeans during summer in Ohio. In unstable conditions (Fig. 1), T and q are highly correlated at the frequencies associated with the flux-carrying eddies. Likewise, the correlations of T and q with χ are large in magnitude, but are negative because the direction of ozone vertical flux is downward, opposite to that for heat and water vapor. In stable conditions with heat flux directed downward (Fig. 2), correlations of T with q and χ are negative and positive, respectively. (Dropoffs at the higher frequencies are mainly due to the effects of sensor separations and the lag time inherent in the ozone sensor.) Apparently, a high degree of similarity between ozone and T or q fluctations and thus between vertical transport properties of the scales can be inferred, as discussed above. By inductive arguments, this

similarity should extend to other scalar quantities such as SO_x, NO_x and fine particles, at least for a height of several meters in the equilibrium boundary layer over relatively short vegetation. This partially justifies the assumption that the eddy diffusivities, as well as normalized cospectra with w, are identical for many scalar quantities. However, for species highly reactive in air and for particles large enough to be significantly affected by gravitational settling these assumptions are not necessarily valid, because the concentrations of these eddies might be significantly altered by processes not considered in this presentation.

References

Wesely, M. L., and B. B. Hicks, 1977: Some factors that affect the deposition rates of sulfur dioxide and similar gases on vegetation, J. Air Pollut. Control. Assoc. 27, 1110-1116.

Wesely, M. L., J. A. Eastman, D. R. Cook, and B. B. Hicks, 1978: Daytime variations of ozone eddy fluxes to maize, Boundary-Layer Meteorol. 15, 361-373.

DEVELOPMENT OF MICROCOMPUTER SYSTEMS IN THE ATMOSPHERIC PHYSICS SECTION

T. J. Martin

A number of microcomputer-based data acquisition and control systems have been implemented in support of the research activities of the Atmospheric Physics Section. This report summarizes the hardware and software developed and describes three systems in use.

Hardware

A commercially manufactured modular microcomputer system was chosen for its range of support products, compactness, adaptability, and low cost. An 8-bit 6809 system was selected for its range of instructions, multiple interrupt capabilities, and size. Usual implementations consume enough power to require a 110 VAC electrical line.

The selected manufacturer produces a range of products including analog-to-digital and digital-to-analog systems, serial and parallel interfaces, timer boards, arithmetic processing units, and prototyping modules, all designed on a small 4 $\frac{1}{2}$ by 6 $\frac{1}{2}$ in 44 pin board. The size of the required enclosure can be varied to suit the application, or single board systems may be used. Development of systems for interfacing with varied experimental apparatus is accomplished in a straightforward manner using prototyping boards manufactured with computer bus interface circuitry.

Software

To date, all software has been developed with a miniassembler/disassembler supplied by the hardware manufacturer. Only machine mnemonics are allowed; no assembler labels are possible. Program storage during the development phase uses a digital cassette tape system. Data fill and move operations are available for performing program changes. Program breakpoint features are available for run-time debugging. The addressing mode features of the 6809, including position-independent code, ease the program development task. The group has recently purchased a cross-software package for use with existing in-house minicomputer systems, to aid in further program development tasks. The focus of the current software

development task has been to create widely applicable routines for use under varied situations.

A general purpose set of input/output and timing routines make up the main system functions. A 10 Hz system clock is implemented for time and task scheduling functions. Routines for software-based 40 bit floating point calculations allow nine decimal digit accuracy with an exponent range of plus or minus 38. These include input/output routines, integer/floating conversion, as well as the four basic arithmetic operations. When trigonometric or other functions are desired, a hardware-based arithmetic processor board is used allowing for 16 and 32 bit integer operations, as well as 32 bit floating operations that yield a digital accuracy of 7 decimal points and an exponent range of ±19. Software for driving this board has been developed for flexible use.

Applications

The final data acquisition and control programs are put into non-destructive 2 K byte EPROM memory. No disk or tape program storage device is required. Normal applications use the general purpose system input/output and timing EPROM, as well as an EPROM containing the application specific control program. When floating point arithmetic functions are desired, an additional EPROM is used.

A system for controlling one or two electrical aerosol analyzers has been created to allow for varying particle scan sequences. An integrating voltage/counter interface measures signal averages over selectable time periods. Output results are printed on a portable terminal and may be stored on cassette tape as well. The computer system consists of three small boards: CPU/memory, dual serial interface, and system clock/experiment interface.

The atmospheric field measurement programs of the Section frequently require variance/covariance computing capabilities. A system has been created to perform continuous calculations on a number of channels at a selectable sampling rate. Hard copy output of mean, variance and covariance results is produced at desired intervals. In addition, these results can be stored on cassette tape, or the raw channel data can be stored for subsequent study such as spectrum analysis. The computer system consists of five boards:

CPU/memory, dual serial interface, one 8-or 16-channel 12 bit A/D arithmetic processor, and system clock.

A stand-alone sodar echo-intensity logger has been designed to operate unattended as slave to a sodar receiver system. A conventional display of height, time and echo intensity is created using a commercially available dot matrix thermal printer with graphics capabilities. A 3x3 matrix of dots produces a gray-scale echo intensity map (see Martin, 1980). As slave, the system automatically creates an echo map to a maximum height of 1500 meters or as allowed by the sodar system. Pulse averaging, selectable offset, and gain adjustments can all be controlled during operation. Date, time, ten minute ticks, height scale, and system parameters are printed out automatically as desired. The system is programmed to restart after power failure and consists of three boards: CPU/memory, serial interface, and system clock/sounder interface.

Reference

Martin, T. J., 1980: Sodar intensity display techniques, Argonne National Laboratory Radiological and Environmental Research Division Annual Report ANL-80-115 Part IV, pp. 14-17.

CALIBRATION OF THE OPEN-FRAME HEAT FLUX DEVICE IN SNOW

D. R. Cook

A thermopile device was recently designed for the measurement of heat flux density in snow (Cook, 1981), possibly for use in studies of dry deposition where a surface energy balance is measured. It is an open-frame design that permits unimpeded flow of heat, water vapor and liquid water. Three of these devices were calibrated in shallow (8 to 15 cm) snows of varied density. The heat flux density in the snow was calculated from

$$\text{Flux} = \lambda(\Delta T/\Delta z_m), \tag{1}$$

where λ is the thermal conductivity of snow and ΔT is the temperature difference across a snow layer of thickness Δz_m in which the open-frame device lies. Temperature measurements were made with iron-constantan thermocouples.

Since direct determination of λ is difficult, the heat capacity C of the snow was measured and then λ determined as

$$\lambda = \left| C \frac{\Delta T_m \Delta z_m \Delta z_{ab}}{\Delta t(\Delta T_a - \Delta T_b)} \right|, \tag{2}$$

where $\Delta T_m/\Delta t$ is the change of mean temperature with time in the layer of snow, and ΔT_a and ΔT_b are the temperature gradients in the snow layers immediately above and below the device, respectively, with Δz_{ab} being the snow thickness over which those temperatures are measured. Snow heat capacity was found from measurements of snow density ρ_s at the level of the open-frame device (the mass of the snow in a container of known volume allowed determination of ρ_s). An eyeball estimate of the percentage of water in the snow was made and then C was calculated from

$$C = \chi_w C_w + \chi_i C_i + \chi_a C_a, \tag{3}$$

where χ_w, χ_i and χ_a are the volume fractions of water, ice and air in the snow, respectively, and C_w, C_i and C_a are the heat capacities of water, ice and air, respectively.

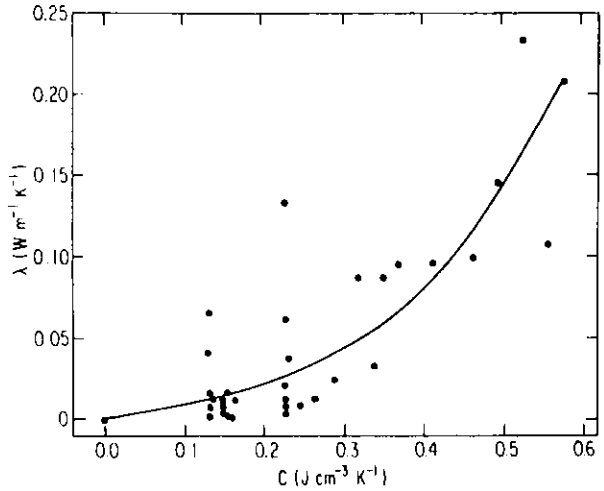

Fig. 1. Thermal Conductivity (λ) versus heat capacity (C) for snow.

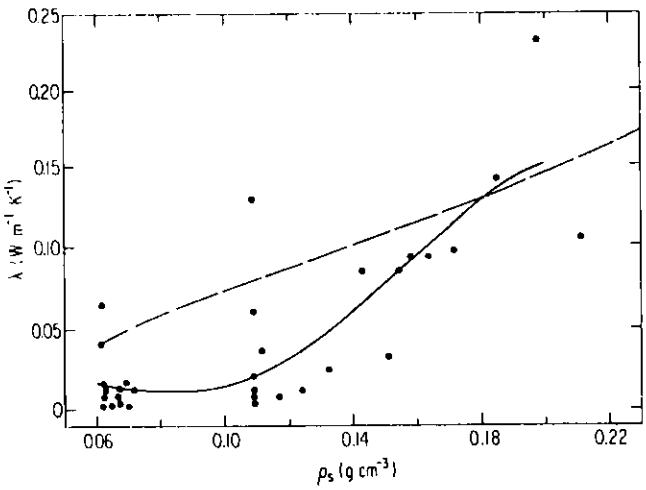

Fig. 2. Thermal Conductivity (λ) versus snow density (ρ_s) for snow.

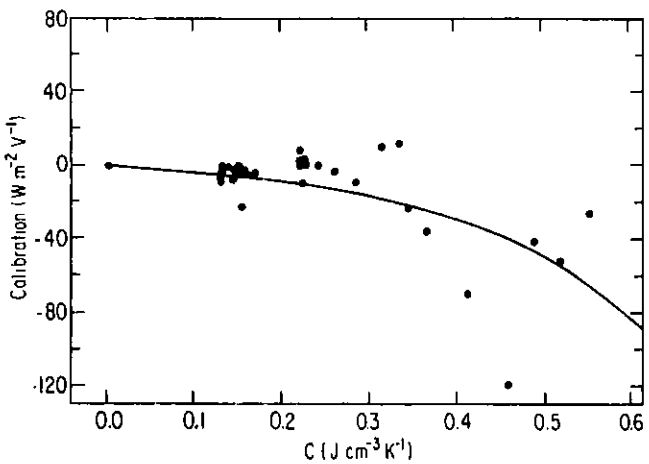

Fig. 3. Average Calibration of the open-frame device versus snow heat capacity (C).

The relationship found between λ and C is shown in Fig. 1. The solid curve is an empirical fit represented by

$$\lambda = 1.38 \times 10^{-2}[\exp(4.78C) - 1], \qquad (4)$$

for λ in W m^{-1} K^{-1} and C in J cm^{-3} K^{-1}. Measurements were made at various time intervals to allow evaluation of measurement procedures. Snow density varied from 0.05 to 0.22 g cm^{-3}. Thermal conductivity and ρ_s are compared in Fig. 2. The solid curve is a polynomial fitted to the data and is represented by

$$\lambda = -7.87 \times 10^{-4} + 2.23 \times 10^{-3}(\rho_s) - 55.3(\rho_s) + 456(\rho_s)^3 - 1067(\rho_s)^4. \qquad (5)$$

The dashed curve approximates the averaged results found by others (List, 1971), and suggests that the calculated conductivities are underestimated. The underestimation is, on the whole, less than the variation of results between investigators. The fluxes measured are very small, between 5 and -5 W m^{-2}, and show a diurnal variation similar to, but of smaller magnitude than, that found in soil (because of the much smaller conductivity of snow).

The open-frame devices were calibrated from the average output of the three devices used. Since it is simpler to determine C than λ, the calibration of the open-frame device is shown as a function of C in Fig. 3. The solid curve is represented by

$$\text{Calibration (W } m^{-2} V^{-1}) = -4.77[\exp(4.74C) - 1]. \qquad (6)$$

This equation may be a slight underestimate because of the possible underestimation of λ. By making simple measurements of ρ_s, the open-frame device is thus calibrated for measured C. Equation (4) can then be used to determine λ.

References

Cook, D. R., 1981: The Open-Frame Heat Flux Plate — A New Design, Radiological and Environmental Research Division Annual Report, Part IV, ANL-80-115, pp. 79-81.

List, R. J., (Ed.), 1971: Smithsonian Meteorological Tables, Smithsonian Institution Press, Washington, DC, p. 404, Table 121.

NITROGEN FIXATION BY LIGHTNING ACTIVITY IN A THUNDERSTORM

D. Drapcho[+], D. L. Sisterson, and R. Kumar[+]

Atmospheric nitrogen fixation by lightning has been estimated from theoretical calculations and laboratory simulations. Considerable debate has occurred in the literature concerning the extent to which this process may affect the global NO_x budget; however, no reports documenting the actual production of NO_x by lightning in the atmosphere had been published until the tentative results of Reiter (1970) and the more recent measurements of Noxon (1976, 1978). In this report, we present experimental evidence for the production of NO_x by an individual flash of cloud-to-ground lightning, as well as by the averaged effect of numerous lightning flashes in the well-mixed air mass in the wake of thunderstorms.

Concentrations of NO and NO_2 were measured continuously over a 48-hour period from April 8 to 10, 1981 in an ambient NO_x monitoring test at Argonne National Laboratory. The nitrogen oxides were monitored with a chemiluminescent NO_x analyzer built by the Environmental Chemistry Group. Early in the two-day period a fairly intense thunderstorm passed over Argonne. Meteorological parameters and O_3 concentrations were available from routine measurements at the Atmospheric Physics Section's meteorological site located 1.3 km SSW of the NO_x sampling site. In addition, detailed observations of storm activity during this thunderstorm were recorded for a different project (Raynor, 1982). This unique set of simultaneous air quality and meteorological data has provided convincing evidence for the production of NO_x by an individual lightning flash and has enabled us to estimate the quantity of NO_x produced.

In the early evening of April 8, 1981, a cold front with associated thunderstorms approached the Argonne area. Air quality and meteorological data taken during the pre-frontal thunderstorm and the frontal passage are presented in Fig. 1. At approximately 2021 CST, the leading edge of a small but intense thunderstorm cell passed from WSW to ENE over Argonne. There was

[+]Environmental Chemistry Group, Chemical Technology Division

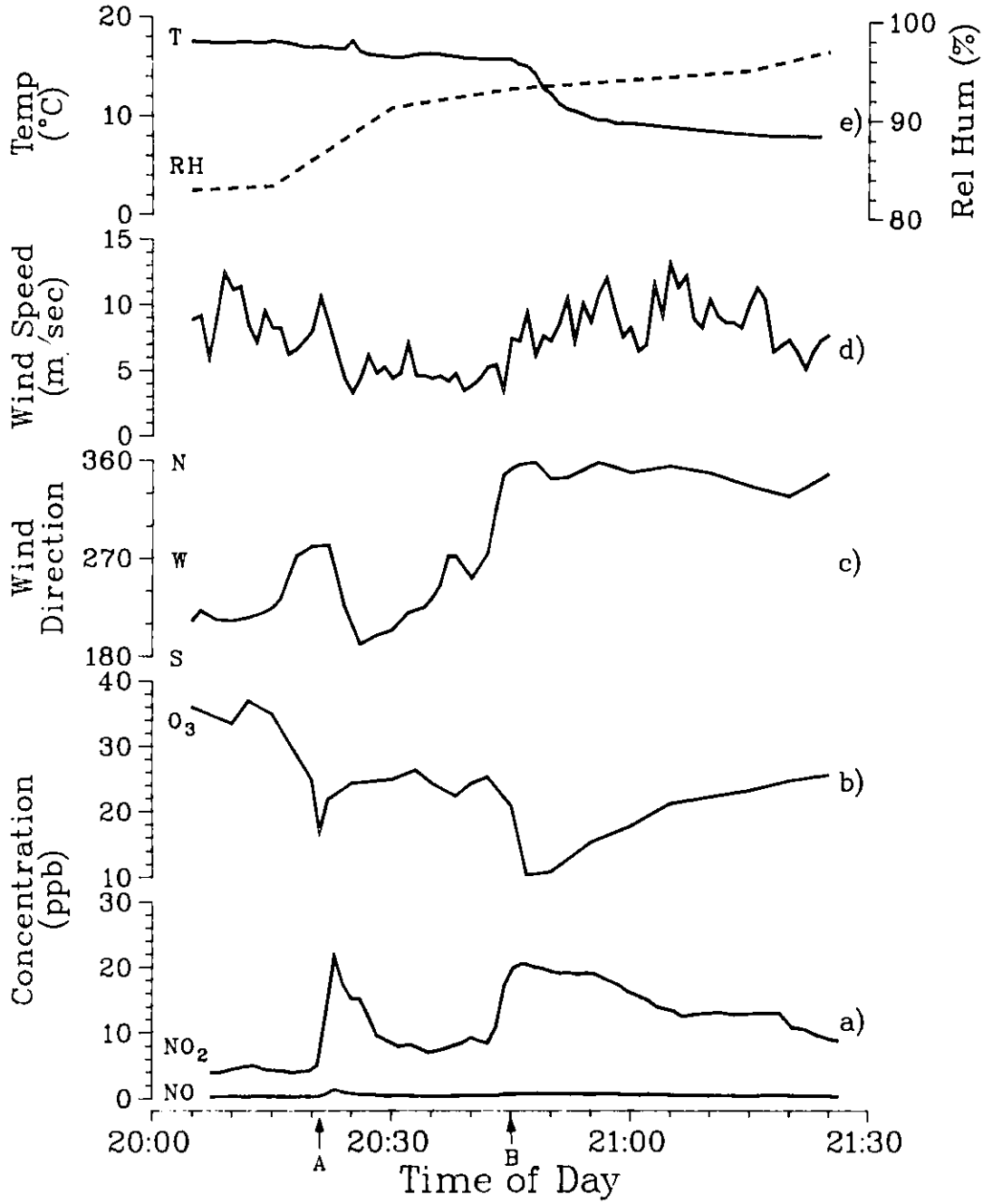

Fig. 1. Temporal patterns during the evening of April 8, 1981 for: a) concentrations of NO and NO_2; b) concentration of O_3; c) wind direction; d) wind speed; and e) ambient surface temperature and relative humidity. Arrow A indicates the time at which the nearby lightning flash was observed. Arrow B indicates the time of the frontal passage.

frequent cloud-to-ground lightning NW through NE of the area at a distance of several kilometers as determined from the time interval between the flash and the corresponding thunder. The intense, local lightning activity lasted only a few minutes and the heavy rain (5 mm in 2 min) tapered off to light rain showers.

One flash was observed about 0.5 km WNW of the meteorology building when the local winds were from the WNW at 10 m s^{-1}, and the air column surrounding the flash was advected over the meteorology site. The wind then decreased sharply from ~11 to ~3 m s^{-1} as it shifted to the S. During this windshift, a small warm temperature spike occurred as relative humidity steadily increased. These meteorology features have been interpreted as indicating that the updraft region of the storm cell passed just to the south of the meteorology site, causing a shift in the local winds, drawing the air column initially surrounding the lightning flash over the meteorology site. The storm continued its ENE movement, drawing the air column toward the NO_x monitoring site a short time later. At this time, a large increase in NO_x concentration was observed. The production rate of NO_x by this lightning flash was estimated from the assumption of a 3 km long instantaneous vertical line source of NO_x from the lightning flash, which gradually expanded into a 700 m diameter column, based upon the horizontal dispersion coefficients of the Pasquill-Gifford stability classification for highly unstable atmospheric conditions (Turner, 1970), with a concentration of 15 ppb (Drapcho et al., 1982), leading to a calculated NO_x production rate of 4×10^{26} molecules/flash.

An intriging feature of the storm event data is the large negative correlation observed between NO_2 and O_3 shown in Fig. 1. The correlation coefficient between O_3 and NO_2 concentrations, taking into account the time lag due to the distance between the two gas analyzers, is -0.85. In earlier work, it was estimated that lightning should produce approximately equal amounts of NO and O_3 (Griffing, 1977). However, our data indicate an approximate 9:10 ratio between ambient ozone decrease and NO_2 increase, indicating little production of O_3 by lightning. Hill et al. (1980) kinetically modeled the production of O_3 by lightning and concluded that lightning only produces NO, with NO_2 formed as a product of the reaction between NO and ambient O_3.

At 2045 CST, the cold front passed over Argonne, as indicated by the wind shift and the temperature decrease. Frequent distant lightning activity was observed in all directions. Again, the NO_x concentration increased corresponding to the frontal passage. This activity continued for some time after the frontal passage. Because of the rapid mixing of air due to the thunderstorm activity, both along and behind the cold front, the air over Argonne now probably represented the area-averaged effects of the numerous lightning strokes.

Our estimate compares favorably with previous estimates of 10^{26} (Noxon, 1976) and 4×10^{26} (Griffing, 1977) molecules/flash. Our value of 4×10^{26} molecules/flash yields an estimate of the global production rate of NO_x by lightning of 30 T_g N yr^1, to be compared with previous estimates ranging from 2 (Hill et al., 1980) to approximately 40 T_g N yr^{-1} (Chameides et al., 1977). Global anthropogenic emissions of NO_x are estimated to be 15 to 20 T_g N yr^{-1} (Burns and Hardy, 1975), indicating that lightning-produced NO_x is likely to be comparable to anthropogenic sources on a global basis.

References

Burns, R. C. and R. W. Hardy, 1975: Nitrogen fixation in bacteria and higher plants, Springer-Verlag, New York.

Chameides, W. L., D. H. Stedman, R. R. Dickerson, D. W. Rusch, and R. J. Cicerone, 1977: NO_x production in lightning, J. Atmos. Sci. 34, 143-149.

Drapcho, D., D. Sisterson, and R. Kumar, 1982: Nitrogen fixation by lightning activity in a thunderstorm. Submitted to Atmos. Environ.

Griffing, G. W., 1977: Ozone and oxides of nitrogen production during thunderstorms, J. Geophys. Res. 82, 943-950.

Hill, R. D., R. G. Rinker, and H. D. Wilson, 1980: Atmospheric nitrogen fixation by lightning J. Atmos. Sci. 37, 179-192.

Noxon, J. F., 1976: Atmospheric nitrogen fixation by lightning. Geophys. Res. Lett. 13, 463-465.

Noxon, J. F., 1978: Tropospheric NO_2, J. Geophys. Res. 83, 3051-3057.

Reiter, R., 1970: On the causal relation between nitrogen-oxygen compounds in the troposphere and atmopsheric electricity, Tellus 22, 122-135.

Raynor, G. S., 1982: Design and preliminary results of the intermediate density precipitation chemistry experiment, Preprints of the Third Joint Conference on Applications of Air Pollution Meteorology, January 11-15, 1982, San Antonio, TX, pp. 47-49.

Turner, D. B., 1970: Workbook of Atmospheric Dispersion Estimates, Air Resources Field Research Office, Environmental Science Services Administration, EPA Office of Air Programs, Research Triangle Park, NC.

ANALYSIS OF DEPOSITION PATTERNS ASSOCIATED WITH EMISSION REDUCTION LEGISLATION

J. D. Shannon

Analysis of past trends or prediction of future trends in pollutant deposition is fraught with uncertainty, as either historical records or future expectations are required for both meteorological and emission variables. As a rule, uncertainty in emission data increases with departure in time from the present. Past meteorology may not be archived in a form convenient for use; future meteorology can be estimated only in the sense of climatological norms or ranges. In addition, in a particular season or year the long-term trend may be markedly reduced or even reversed. For example, even for doubled emissions there is little wet deposition during a drought. Trend analyses can easily be misused unless the uncertainties are understood.

Two legislative bills recently introduced on the issue of curbing emissions related to acid deposition, the Mitchell and Moynihan bills, call for reductions of approximately 45 and 37%, respectively, in the eastern U.S. The Congressional Office of Technology Assessment (OTA) requested an examination of the deposition reduction associated with the emission reduction, and the Advanced Statistical Trajectory Regional Air Pollution (ASTRAP) model (Shannon, 1981) was exercised for the requested simulations.

Table 1. January-July sulfur deposition budget, kT S units

	Emissions	Deposition in U.S.	Deposition in Canada
Eastern U.S. (current)	1950	1020	200
Moynihan bill	1230	610	130
Mitchell bill	1070	540	110

The simulations are summarized in Table 1 and illustrated in part in Fig. 1; since OTA could provide estimated future emissions only on a statewide basis, "hot spots" associated with individual large sources are necessarily

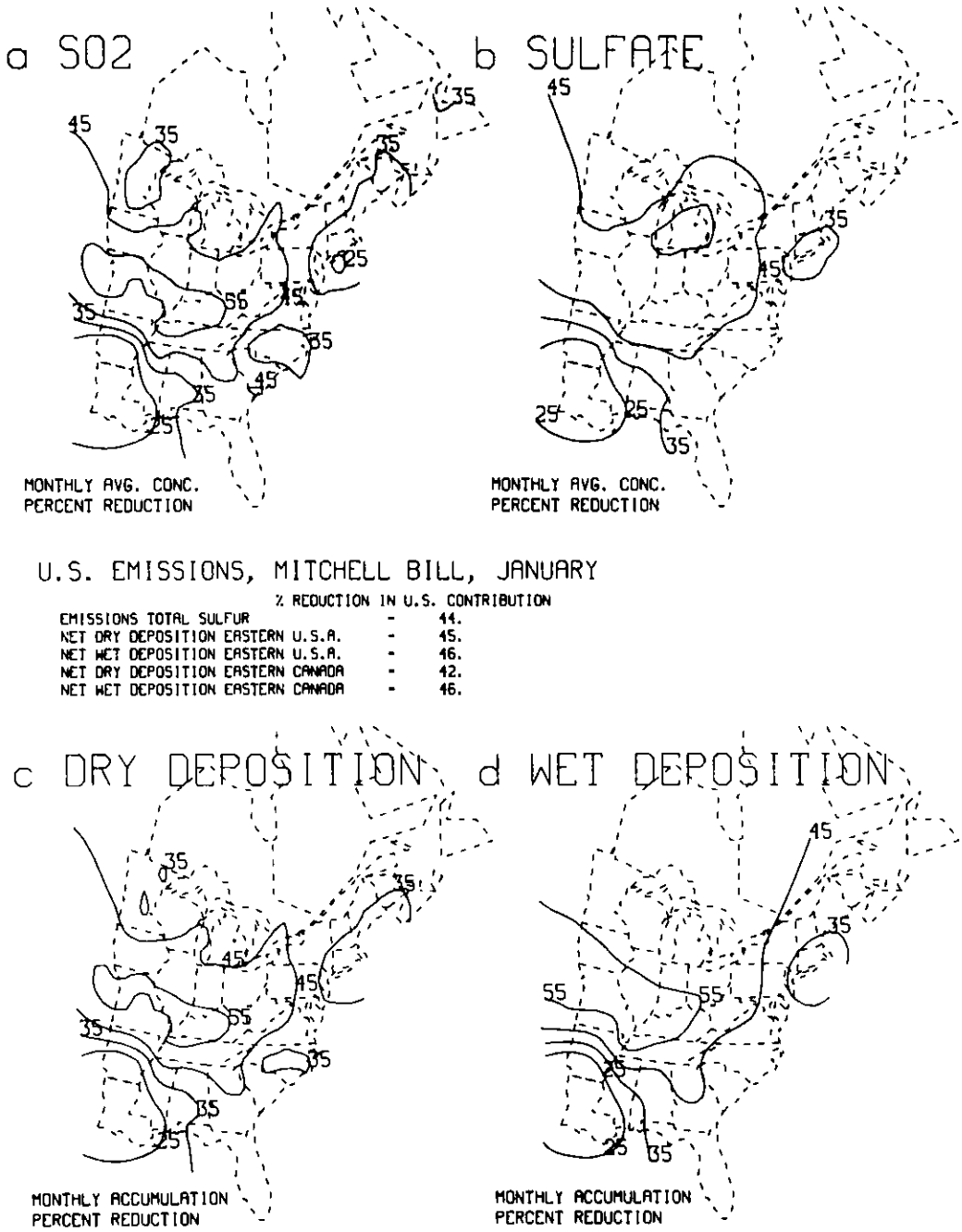

Fig. 1. Percentage reduction in the U.S. contribution to pollutant sulfur concentrations and deposition associated with the Mitchell bill.

smoothed out. The overall sulfur deposition reductions in ASTRAP simulations correspond quite closely to the emissions reductions. It is clear that simulations covering more meteorological periods should be prepared. Unresolved questions, which will require considerable future research, deal

with determination of the relationship between total acid deposition and total sulfur deposition, and understanding of whether a radically different pollutant mix can still be modeled successfully by the linearized parameterizations, used in models such as ASTRAP that have been developed from field studies with the current pollutant mix.

Reference

Shannon, J. D., 1981: A model of regional long-term average sulfur atmospheric pollution, surface removal, and net horizontal flux, Atmos. Environ. 15, 689-701.

FORMATION OF SULFATE IN A CLOUD-FREE ENVIRONMENT

I.-Y. Lee

A sulfate aerosol model that simulates homogeneous gas kinetics via 23 chemical reactions involving 19 species, particle growth by coagulation and heteromolecular diffusion, and solar radiation effects has been developed to examine the microphysical mechanisms associated with clear-air transformation of sulfur dioxide to sulfates in the lower troposphere. The chemical kinetics model in this study is a version of the model of Swan and Lee (1980), modified to include SO_x reactions. In general, the kinetics model consists of two groups, NO_x reactions and SO_x reactions. However, the chemical processes of the SO_x group cannot proceed independently owing to the participation of free radicals in both groups. A flow diagram (Fig. 1) shows the role of free radicals in the present version of the model. Here, we see clearly the contributions by free radicals OH and HO_2 (in the middle of Fig. 1) to NO_x and SO_x chemistry. From this diagram, we also notice that the oxidation of SO_2 depends on insolation since OH is produced mainly by photolysis of HNO_2, and that the production of gas-phase H_2SO_4 is controlled by the available moisture content in air. With gas-phase photochemical reactions included, the model evaluates the rate of formation of particles, actually droplets of sulfuric acid solution, and continuously adjusts the particle size spectrum in accordance with microphysical processes of condensation and coagulation.

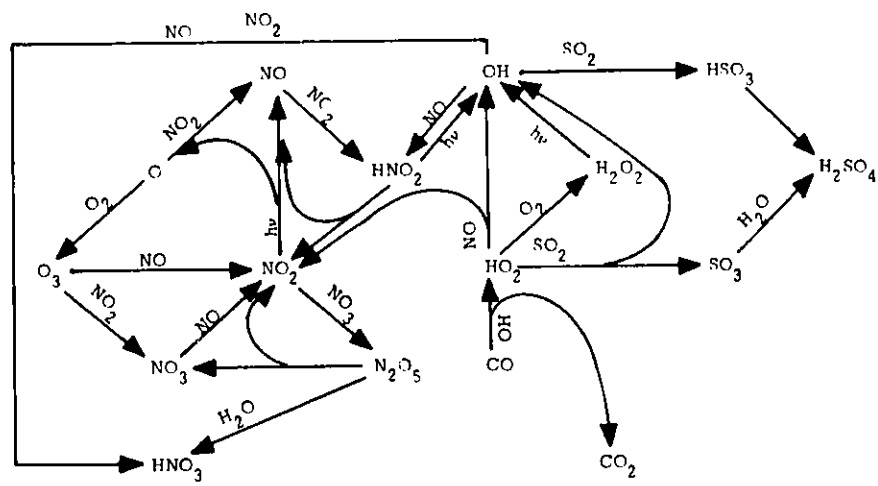

Fig. 1. Flow diagram of the present version of the chemistry model.

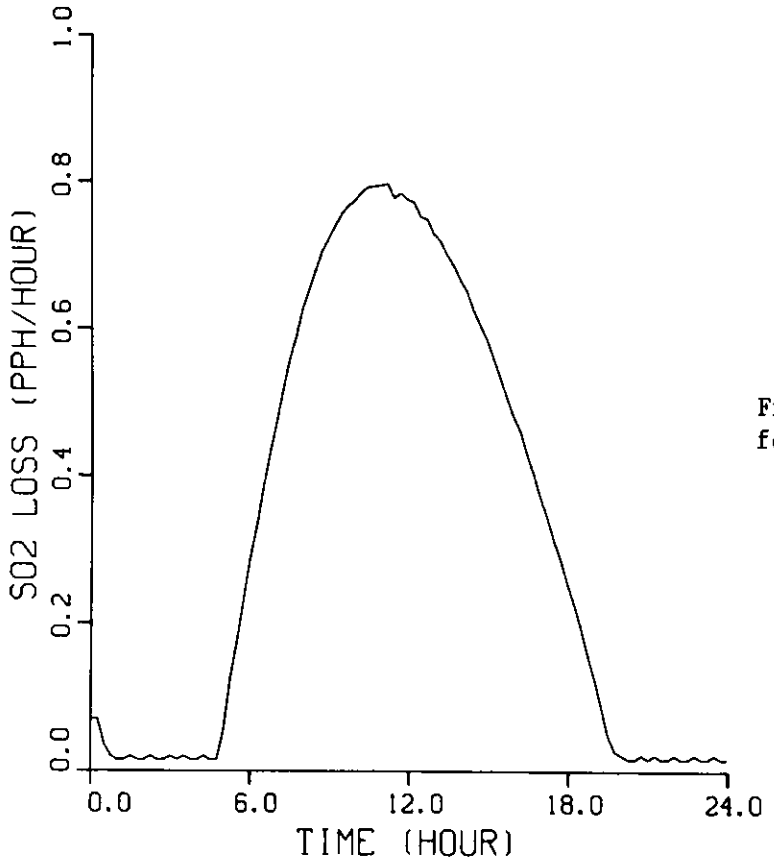

Fig. 2. Clean-air transformation rate of SO_2.

The temporal variations of the oxidation rate of SO_2 and size distribution of sulfate aerosol have been computed with specified initial concentrations and assumed atmospheric conditions of 100% of available insolation (no clouds) and 50% relative humidity. The oxidation rate of sulfur dioxide undergoes a diurnal cycle (Fig. 2), reaching a maximum of 0.8% hr^{-1} at 1100. The spectral evolution of H_2SO_4 solution droplets reaches steady state by late afternoon with a bimodal distribution consisting of an active mode at 0.03 μm radius and an inactive mode at 0.0004 μm (Fig. 3). Volume distributions have been computed (Fig. 4) with various preexisting distributions of urban and continental background aerosols provided from previous work (Lee et al., 1980) with some modifications. The magnitude and mode of the volume distribution computed with urban aerosols compare favorably with those observed during a recent St. Louis plume experiment (Komp et al., 1978), not shown.

Additional conditions used to examine the sensitivity of transformation of sulfur dioxide and production of particulate sulfates to

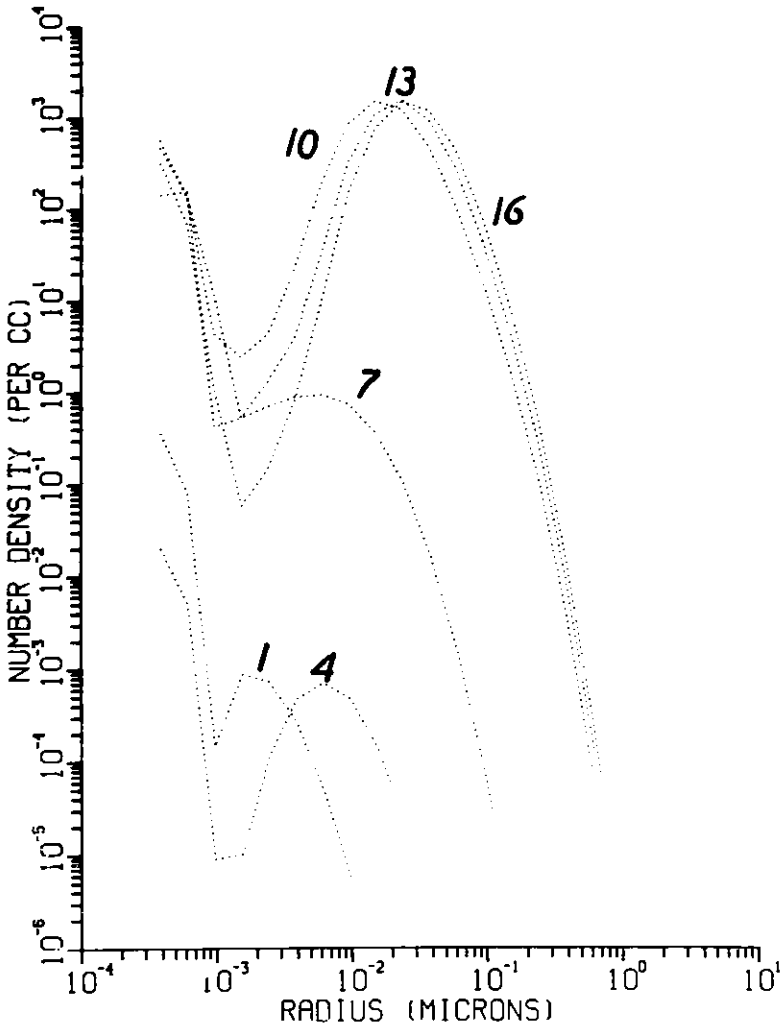

Fig. 3. Spectral evolution of sulfate particles. In this figure, the curves represent the particle distribution, a plot of the number of sulfate particles in each given size bin, after 1, 4, 7, 10, 13, and 16 hr of simulation without preexisting aerosol particles.

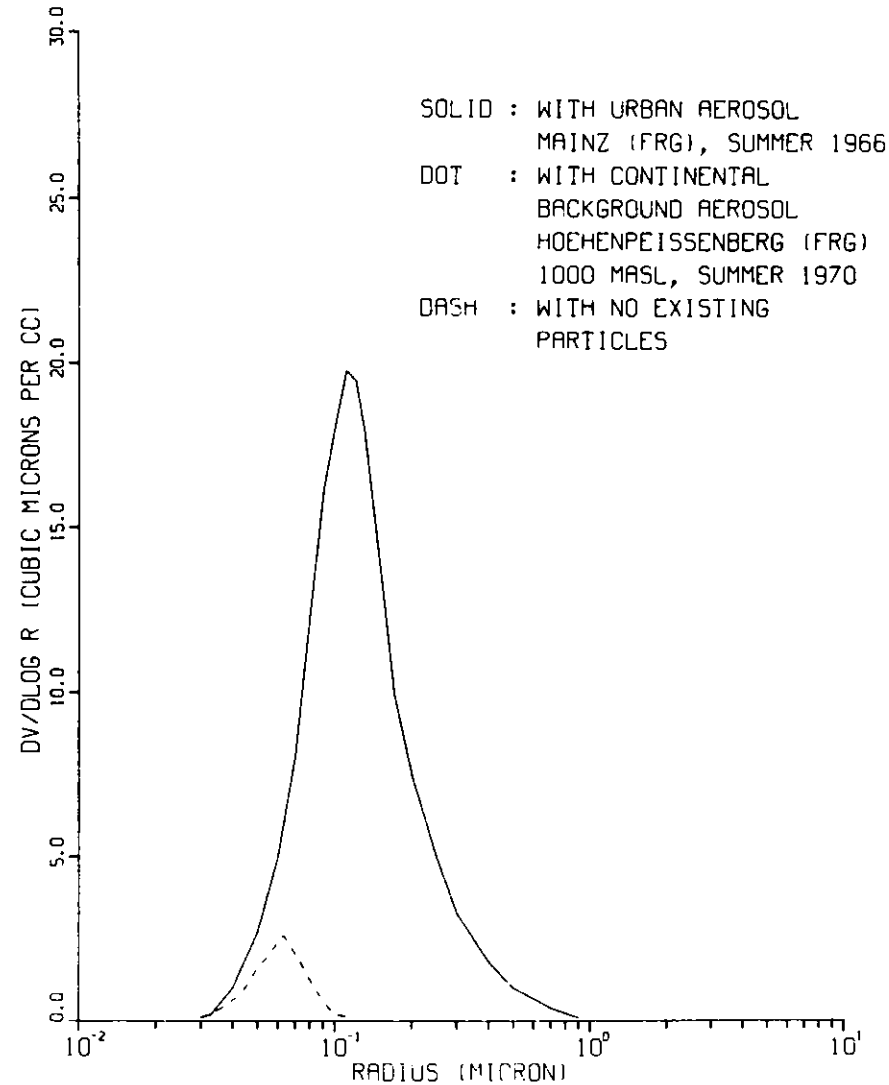

Fig. 4. Volume distributions computed with preexisting urban and continental background aerosol particles.

Table 1. Comparison of model simulations with different atmospheric conditions.

Case	Relative insolation, %	Relative humidity, %	Mode concentration cm^{-3}	Maximum transformation rate of SO_2 % hr^{-1}	Average transformation rate of SO_2, % hr^{-1}
A.1	50	90	4200	0.52	0.23
A.2	75	90	4800	0.67	0.29
A.3	100	90	5200	0.81	0.35
B.1	100	70	4900	0.80	0.34
B.2	100	50	1600	0.80	0.34

solar insolation and relative humidity are summarized in Table 1. In general, the active mode of the spectrum consists of particles of radius between 0.02 and 0.03 μm. We see that the transformation rate of SO_2 and the mode concentration both increase rapidly with increasing insolation. On the other hand, only the number concentration increases with increasing relative humidity, and the oxidation rate of SO_2 is little changed.

References

Komp, M. J. and A. H. Auer, Jr., 1978: Visibility reduction and accompanying aerosol evolution downwind of St. Louis, J. Appl. Meteorol. 17, 1357-1367.

Lee, I.-Y., G. Hänel and H. R. Pruppacher, 1980: A numerical determination of the evolution of cloud drop spectra due to condensation on natural aerosol particles, J. Atmos. Sci. 37, 1839-1853.

Swan, P. R. and I.-Y. Lee, 1980: Meteorological and air pollution modeling for an urban airport, J. Appl. Meteorol. 19, 534-544.

SIMULATION OF TRANSPORT AND REMOVAL PROCESSES OF SAHARAN DUST

I.-Y. Lee

Large quantities of dust particles are injected into the atmospheric boundary layer over the Saharan region of North Africa. Strong surface heating over the Sahara region of North Africa creates sufficient convective instability to generate a deep mixed layer, into which large quantities of dust particles are injected. When this hot and dry air emerges from the west coast of North Africa, a strong inversion at the interface between the Saharan air layer (SAL) and the marine layer inhibits entrainment of the dust particles into the lower layer; the Sarahan dust is transported across the Atlantic on the equatorial side of the persisting subtropical high.

To understand the evolution of dust particles in terms of dynamic and microphysical processes, a planetary boundary layer (PBL) model (Lee and Swan, 1977) has been modified to include three layers: PBL, SAL and free atmosphere. The processes of particle sedimentation and coagulation have been incorporated (Turco et al., 1979), and computations have been carried out for a selected trajectory in the SAL.

The model was used to simulate behavior for two weeks in July (10 to 24 July). The fields of PBL and SAL dust concentration at 1800 GMT July 24 are presented in Fig. 1 and 2. In general, dust particles from the Sahara desert are transported along the northeasterly wind and then follow the southeasterly wind after passing the ridge. Dust particles in the SAL reach Barbados (15°N, 60°W) in two weeks. In the PBL, however, most of the particles are removed within 1000 km of the African coast.

As an air parcel moves along the a trajectory, variations in particle spectra (e.g., volumetric mixing ratio versus particle radius) occur by diffusion, coagulation and sedimentation. Figure 3 shows the evolution of spectra computed for several days along the trajectory shown in Fig. 2. The concentration of dust particles decreases markedly with time, particularly particles larger than 10 μm in diameter. That is, large particles are produced by coagulation and removed by gravitational sedimentation. In a simulation without coagulation, the mode of large particles disappeared completely within two days.

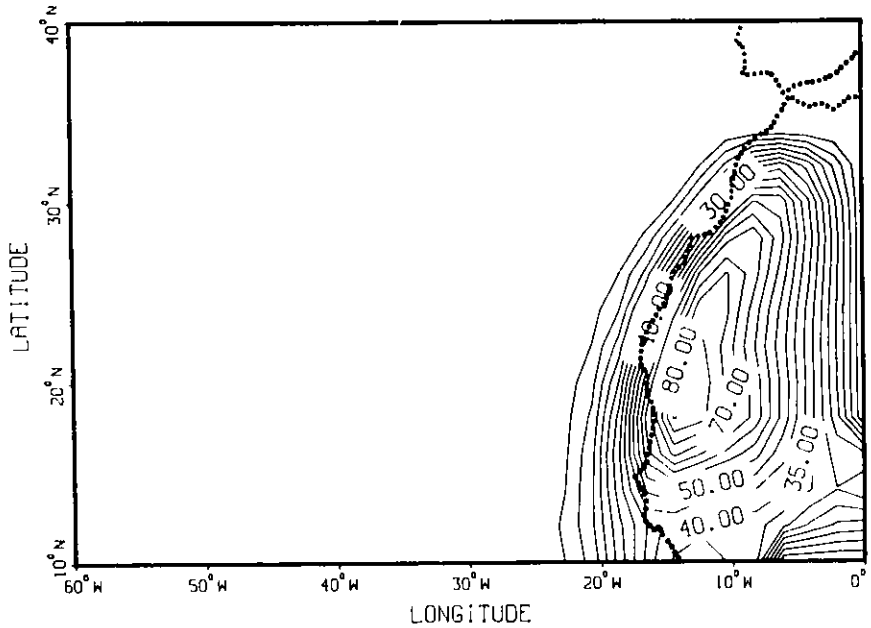

Fig. 1. Normalized dust concentration field in the PBL at 1800 GMT (at 30° W) on July 24.

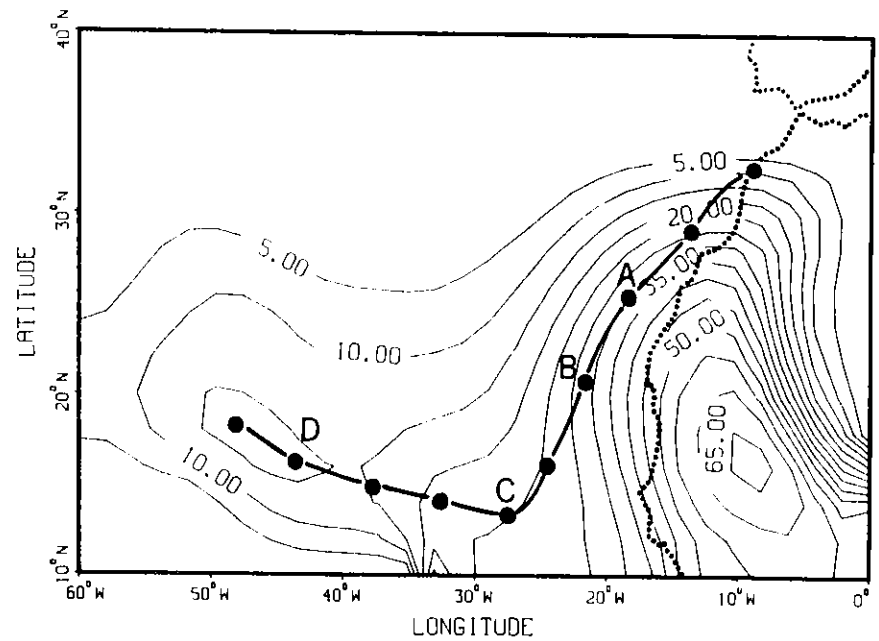

Fig. 2. Normalized dust concentration field in the SAL at 1800 GMT (at 30° W) on July 24, and a selected parcel trajectory.

This preliminary study demonstrates that the fate of Saharan dust particles can be simulated by combining processes of long range transport and microphysics of coagulation and sedimentation. The computed value of dust volume compares favorably with observations made by Prospero and Carlson (1972) near Barbados.

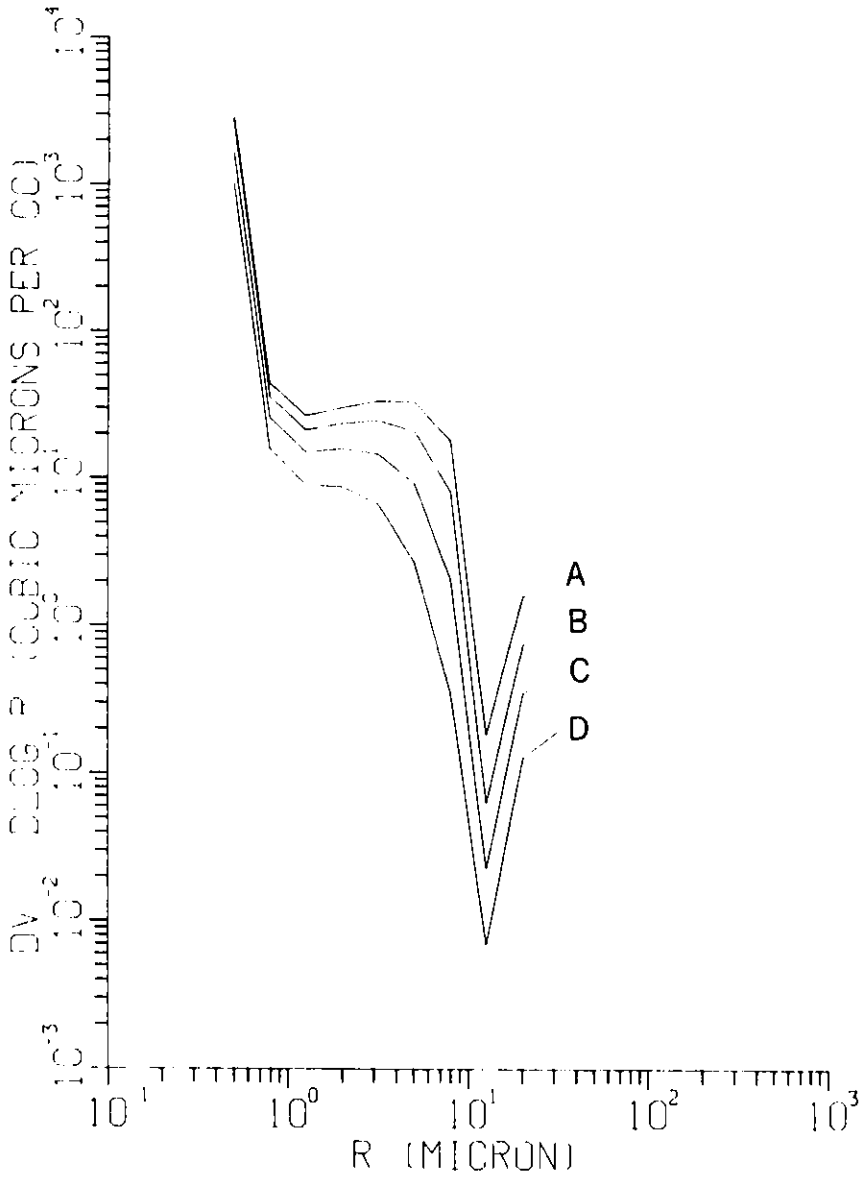

Fig 3. Volume distribution obtained after two (A), three (B), five (C), and eight (D) days.

References

Lee, I. Y. and P. R. Swan, 1977: Transport of contaminants in the planetary boundary layer, Preprints, of the Joint Conf. on Applications of Air Pollution Meteorology, Salt Lake City, pp. 392-399.

Prospero, J. M. and T. N. Carlson, 1972: Vertical and areal distribution of Saharan dust over the western equatorial north Atlantic ocean, J. Geophys. Res. 77, 5255-5265.

Turco, R. P., P. Hamill, O. B. Toon, R. C. Whitten, and C. S. Kiang, 1979: The NASA-Ames Research Center stratospheric aerosol model, NASA Technical Paper 1362.

SEASONAL AND ANNUAL COMPARISON OF WEEKLY AND EVENT SAMPLING OF PRECIPITATION CHEMISTRY

D. L. Sisterson and B. Wurfel

A comparison of event and weekly precipitation chemistry sampling has been completed at Argonne for April 1980 through March 1981. Event samples collected under the Multistate Atmospheric Power Production Pollution Study (MAP3S) protocol and analyzed by the Analytical Chemistry Laboratory at Argonne have been weighted by precipitation amount to produce weekly values and designated ANL samples. Weekly samples collected for the National Atmospheric Deposition Program (NADP) have been analyzed by the Central Analytical Laboratory at the Illinois State Water Survey. Details of the collection and analytical procedures are presented elsewhere (Sisterson and Wagner, 1980; Sisterson and Wurfel, 1980).

During the one-year period, 91 event and 43 weekly samples were collected. Partial samples resulting from collector malfunction and samples with insufficient volumes were not analyzed, reducing the number of event and weekly samples used in this study to 62 and 31, respectively. Integrity of chemical analysis was determined from ion balances

$$\left[\frac{\text{CATIONS} - \text{ANIONS}}{\text{CATIONS} + \text{ANIONS}}\right] \times 100\%,$$

where ±14.0% was considered acceptable. Samples with bad ion balances were reanalyzed, but were included in the study only if their redetermined ion balances were within acceptable limits.

Occasionally, when more than one event occurred during a week, one or more of the samples was too small to be analyzed or had a bad ion balance. A decision to eliminate the entire week from the study was determined on the basis of precipitation amount. If the difference in rain amount between the incomplete event-summed sample and the weekly sample was greater than 2%, the entire week was eliminated. Of the 9 weekly (25 event) samples affected by incomplete sampling, 4 weekly (7 event) samples were eliminated from the data set. Although use of the incomplete event-summed samples may introduce a bias, the samples are included in this preliminary

report. Plots of event-summed versus weekly individual ions were also constructed. Outliers were determined from visual inspection and corresponding samples were eliminated from the comparison study.

Only 27 event and 17 weekly complete samples survived the close scrutiny; selected parameters from the subset summed over seasonal and annual time periods (Table 1) can be compared to the same parameters from the entire "acceptable" data set consisting of the 62 event and 31 weekly samples summed over the one year period (Table 2). Good agreement exists and perhaps justifies assuming that Table 1 is representative of all data collected during the one-year period.

Table 1. Seasonal and annual differences of selected chemical species for complete sample analysis. AVG is [(NADP + ANL)], DIFF is [(NADP - ANL)]/mean] x 100%. There were 5 event and 3 weekly samples for spring, 9 event and 4 weekly samples for summer, 7 event and 5 weekly samples for fall, and 6 event and 5 weekly samples for winter. All values are in μeq/L except where indicated.

	Avg. rain g	Diff	Avg. H^+(pH lab)	Diff	Avg. Ca^{++}	Diff, %
Spring	3377.50	+0.72%	39.94	-30.68%	31.81	+15.54%
Summer	13171.50	+1.12%	73.12	-10.87%	14.31	-5.71%
Fall	3499.95	+5.23%	40.38	-15.46%	17.17	+43.98%
Winter	4820.90	+3.49%	56.54	-12.11%	5.86	+39.71%
Annual	24869.50	+2.14%	60.79	-13.51%	15.47	+11.06%
	Avg. Mg^{++}		Avg. K^+		AVG Na^+	
Spring	10.57	+31.89%	1.53	-52.64%	6.59	+1.35%
Summer	4.05	+19.06%	1.19	-96.55%	2.42	-15.20%
Fall	8.64	+33.09%	1.03	-36.22%	2.53	+14.78%
Winter	1.81	+86.11%	0.11	+200.00%	1.55	+34.58%
Annual	5.15	+30.57%	1.01	-72.60%	2.83	-1.28%
	Avg. NH_4^+		Avg. NO_3^-		AVG $SO_4^=$	
Spring	27.58	-47.25%	32.70	+18.95%	58.79	+11.94%
Summer	24.13	-28.33%	32.00	+4.45%	79.91	+4.83%
Fall	26.00	-21.27%	30.55	+8.96%	60.09	+31.52%
Winter	16.17	-22.62%	20.70	+6.57%	53.26%	+26.00%
Annual	23.33	-29.57%	29.70	+7.43%	70.47	11.88%

	AVG pH lab
Spring	4.40
Summer	4.14
Fall	4.39
Winter	4.25
Annual	4.22

Table 2. Comparison of individual mean event-summed (ANL) and weekly (NADP) precipitation chemistry and acidity parameters where DIFF is [(NADP - ANL)/mean] x 100%. The number of samples summed from April 1980 through March 1981 are in parenthesis. All values are in μeq/L except where indicated.

	H^+ (pH field)	H^+(pH lab)	H^+(pH Gran)	Conductivity (μS/cm)
ANL	59.78 (48)	66.76 (36)	59.88 (43)	34.88 (53)
NADP	53.46 (25)	60.15 (23)	55.04 (23)	33.37 (27)
DIFF	-11.15%	-10.42%	-8.42%	-4.42%

	Ca^{++}	Mg^{++}	K^+
ANL	16.31 (55)	4.88 (55)	1.54 (50)
NADP	17.78 (28)	5.91 (28)	.77 (26)
DIFF	+8.66%	+19.15%	-67.21%

	Na^+	NH_4^+	NO_3^-	$SO_4^=$
ANL	3.50 (54)	29.86 (56)	30.19 (54)	70.43 (54)
NADP	3.13 (27)	22.99 (28)	32.97 (28)	76.45 (27)
DIFF	-5.55%	-25.98%	+8.78%	+8.20%

pH field		pH lab		pH Gran	
NADP	ANL	NADP	ANL	NADP	ANL
4.27 (48)	4.22 (25)	4.22 (23)	4.18 (36)	4.26 (23)	4.22 (43)

The average concentration of H^+ in Table 1 shows precipitation to be most acidic in summer and winter. Generally, $SO_4^=$ average concentrations follow a similar trend but nitrate and ammonium concentrations are uniform. Soil derived ions (Ca^{++}, Mg^{++}, K^+) and Na^+ concentrations are largest in spring, least in summer. The differences between ANL and NADP samples also show seasonal variation not related to average concentrations; i.e., the differences do not appear to be a strict function of concentration. The difference between ANL and NADP H^+ average concentrations are uniform except for spring. The $SO_4^=$ differences are largest in fall and winter; this may be due to $SO_3^=$ (not analytically determined in event samples) being slowly oxidized to $SO_4^=$. This process is usually very rapid but the colder temperatures may retard that process, particularly for event samples. Soil-derived ion (except K^+) differences are least in summer. Since soil-derived materials may slowly dissolve during the weekly collection period, differences would be expected to be large (Peden and Skowron, 1978). Most of the annual

precipitation fell during summer in this study, however, resulting in high soil moisture levels and relatively low atmospheric dust loading then. This could explain, in part, why summer precipitation was more acidic, since the somewhat calcareous soils of northeastern Illinois normally help mitigate precipitation acidity (e.g., Sisterson, 1981a).

Results of this study are not yet complete, since accuracy for each of the laboratories must be included to determine the significance of the differences (e.g., Sisterson, 1981b). These preliminary findings indicate that annual differences between weekly and event precipitation chemistry are relatively small; seasonal differences, however, may be substantial.

References

Peden, M. E. and L. M. Skowron, 1978: Ionic stability of precipitation samples, Atmos. Environ. 12, 2343-2349.

Sisterson, D. L. and D. Wagner, 1980: A comparison of the chemistry of event and weekly precipitation samples in northern Illinois--A preliminary report, Part 2, Argonne National Laboratory Radiological and Environmental Research Division Annual Report ANL-80-115, Part IV, pp. 72-74.

Sisterson, D. L. and B. Wurfel, 1980: A comparison of the acidity of event and weekly precipitation samples in northern Illinois--A preliminary report, Part 1, Argonne National Laboratory Radiological and Environmental Research Division Annual Report ANL-80-115, Part IV, pp. 68-71.

Sisterson, D. L., 1981a. Partial neutralization of rainfall acidity by soil-derived particles in northeastern Illinois, this report.

Sisterson, D. L., 1981b: Accuracy of ANL and NADP precipitation chemistry analyses, this report.

PARTIAL NEUTRALIZATION OF RAINFALL ACIDITY BY SOIL-DERIVED PARTICLES IN NORTHEASTERN ILLINOIS

D. L. Sisterson

Soil-derived particles may play an important role in reducing precipitation acidity. Generally, the most important mineral components of natural windblown dust are quartz, carbonates, feldspars, and clay (Winkler, 1973). Carbonate minerals, such as calcite, can readily react with acids in precipitation (Winkler, 1976). The calcareous soils of northeastern Illinois would, therefore, be expected to play an important role in local precipitation acidity. The greater precipitation acidity in the Northeast may be, in part, a consequence of the underlying igneous and metamorphic rocks, which do not produce acid-neutralizing calcite.

Calcium carbonate, which is abundant in calcareous soils, can react with the strong inorganic acids present in precipitation, as summarized in the following reactions:

$$CaCO_3 + H_2SO_4 \rightarrow CaSO_4 + H_2O + CO_2,$$

and

$$CaCO_3 + 2HNO_3 \rightarrow Ca(NO_3)_2 + H_2O + CO_2.$$

An obvious decrease of acidity during precipitation can result.

An example of partial neutralization of precipitation acidity was believed to have been observed during the multilaboratory OSCAR (Oxidation and Scavenging Characteization of April Rain) experiment in April 1981 under the MAP3S program. This Section operated a sequential precipitation collection site for the intermediate network of OSCAR (Raynor, 1982). Precipitation samples were collected in bottles that were changed after an accumulation of ~ 100 ml, corresponding to 0.6 mm (0.024 inches) of rain. The pH and conductivity patterns of a typical convective storm, the second of three OSCAR events at Argonne, show a decrease in precipitation acidity and ionic strength (conductivity) as the rain rate increases (Fig. 1). The contrasting pH and conductivity patterns of the first OSCAR event, which occurred after a long dry period, are shown in Fig. 2. The National Weather Service reported dust

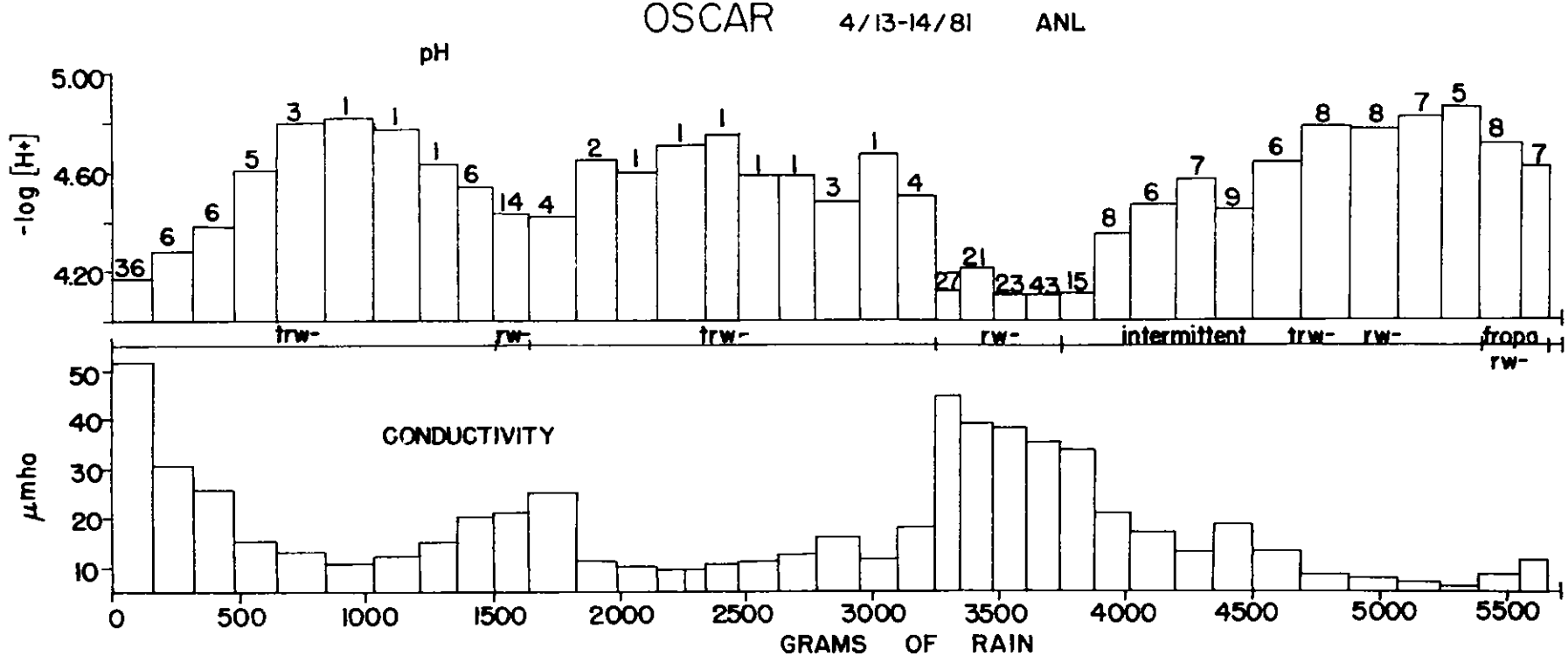

Fig. 1. Determination of pH and conductivity in sequential samples from the second OSCAR event. Collection time in minutes is given above the pH graph; storm type is given below the graph. (Argonne National Laboratory, April 13 and 14, 1981).

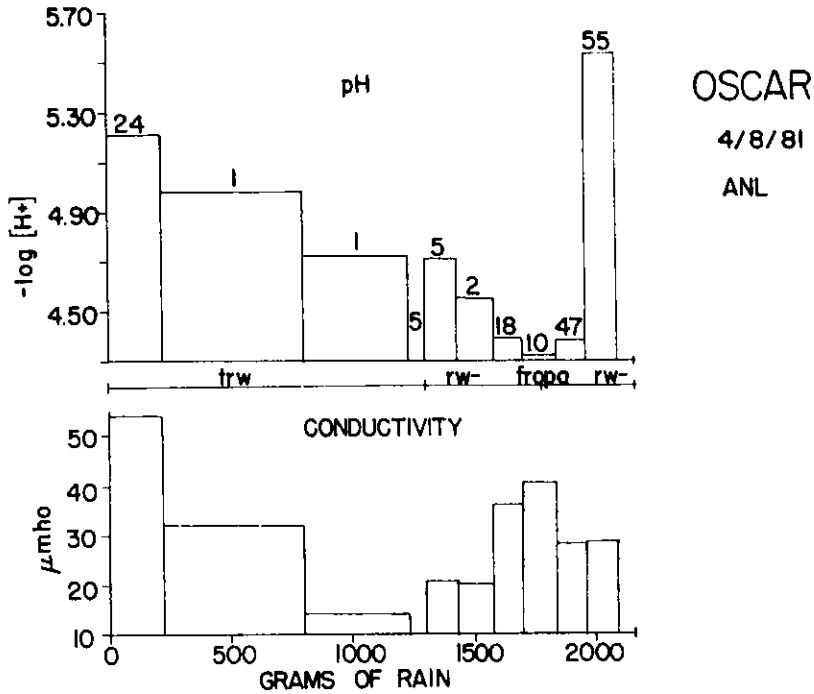

Fig. 2. Same as Fig. 1 except for the first OSCAR event. (Argonne, April 8, 1981).

aloft over northeastern Illinois and the skies were noticeably turbid. In this event, acidity increased as the rain rate increased. While these samples have not yet been chemically analyzed, the first few sequential samples collected were extremely cloudy, similar in appearance to other rain samples collected at Argonne containing high concentrations of soil-derived particles (Ca^{++} and Mg^{++}). Because these particles are relatively large, they are quickly scavenged by precipitation. The high concentration of these particles was apparently sufficient to neutralize most of the acids early in the rain. As the rain continued, most of the neutralizing soil particles were removed, and the precipitation samples became more acidic.

Observed differences between weekly and event precipitation acidity (e.g. Sisterson and Wurfel, 1981) may also be attributed to the effects of soil particles. The same chemical reactions that during precipitation partially neutralize acids may continue within the sample awaiting collection, as well as during storage. Peden and Skowron (1978) have shown that soil-derived ions (Ca^{++}, Mg^{++}, K^{+}) in collected precipitation undisolved dramatic increases in concentration with time and hypothesized that soil particles not yet in equilibrium with the aqueous phase slowly dissolve; an ion exchange mechanism is probably involved, with the soil particles acting as a cation

exchange medium. These effects are most pronounced when the undissolved particulate concentration in collected precipitation samples is highest. Decreasing acidity and increasing concentrations of soil-derived ions in weekly precipitation samples, when compared to event-summed samples is attributed in part to calcium carbonate reacting with the acids prior to weekly collection (e.g., Sisterson and Wurfel, 1980; Sisterson and Wagner, 1980).

References

Peden, M. E. and L. M. Skowron, 1978: Ionic stability of precipitation samples, Atmos. Environ. 12, 2343-2349.

Raynor, G. S., 1982: Design and preliminary results of the intermediate density precipitation chemistry experiment. Preprints of the Third Joint Conference on Applications of Air Pollution Meteorology, Jan. 11-15, 1982, San Antonio, TX.

Sisterson, D. L. and D. Wagner, 1980: A comparison of the chemistry of event and weekly preciptiation samples in northern Illinois -- A preliminary report, Part 2, Argonne National Laboratory Radiological and Environmental Research Division Annual Report ANL-80-115, Part IV, pp. 72-74.

Sisterson, D. L. and B. Wurfel, 1980: A comparison of the acidity of event and weekly precipitation samples in northern Illinois -- A preliminary report, Part 1, Argonne National Laboratory Radiological and Environmental Research Division Annual Report ANL-80-115, Part IV, pp. 68-71.

Sisterson, D. L. and B. Wurfel, 1981: Seasonal and annual comparison of weekly and event preciptation chemistry, this report.

Winkler, E. M., 1973: Stone: Properties, Durability in Man's Environment, Springer-Verlag, New York.

Winkler, E. M., 1976: Natural dust and acid rain, Water, Air, and Soil Pollution 6, 295-302.

ACCURACY OF ANL AND NADP PRECIPITATION CHEMISTRY ANALYSES

D. L. Sisterson

Comparisons of precipitation chemistry and acidity measured in the weekly National Atmospheric Deposition Program (NADP) to that from appropriately weighted weekly sums of event (ANL) precipitation samples began in April 1980 (Sisterson and Wagner, 1980; Sisterson and Wurfel, 1980). Since that time, one complete year of data has been collected and analyzed, the results of which are reported elsewhere (Sisterson and Wurfel, 1981). One of the most challenging aspects of the comparison study has been the determination of whether any bias results from differences in analytical procedures and instrumentation of the Analytical Chemistry Laboratory at Argonne (used for ANL samples) and the Central Analytical Laboratory at the Illinois State Water Survey (used for NADP samples). This report summarizes the bias and precision of each parameter in the comparison study for each laboratory and how this information will be applied to the correction of data used in that study.

ANL samples were analyzed by liquid ion chromatography for Na^+, K^+, NH_4^+, Cl^-, $SO_4^=$, and NO_3^-, and by flame atomic absorption for Ca^{++} and Mg^{++}. NADP samples were analyzed by an autoanalyzer for all the ions above except Ca^{++}, Mg^{++}, K^+, and Na^+ whose concentrations were determined by flame atomic absorption.

Bias is defined as

$$\left(\frac{\text{mean value} - \text{certified value}}{\text{certified value}}\right) \times 100\% , \qquad (1)$$

and precision is defined as

$$\left(\frac{2 \times \text{standard deviation}}{\text{mean value}}\right) \times 100\% . \qquad (2)$$

Precision is a function of concentration and was determined from prepared standards whose values corresponded to the detection limit, median concentration, and high concentration for event and weekly samples collected from April 1980 to March 1981. The detection limit is defined as twice the

Table 1. Bias for median and high concentrations determined from event and weekly precipitation samples collected from April 1980 through April 1981 for the Analytical Chemistry Laboratory (ANL samples) and the Central Analytical Laboratory (NADP samples). Values in brackets were assumed.

	ANL Analyses		NADP Analyses	
Parameter	Value	Bias, %	Value	Bias, %
Precipitation Amount	300 g	0.0	300	+2.0
	1300 g	0.0	1300	+1.5
Titration, μeq/L	40	+14.1	[40	+14.1]
	132	+17.0	[132	+17.0]
pH	[3.06	+3.4]	3.06	+3.4
	[4.08	+4.5]	4.08	+4.5
Conductivity, μS/cm	[35.5	+1.0]	35.5	+1.0
	[401	+0.6]	401	+0.6
Ions, mg/L				
Ca^{++}	0.32	-15.8	0.35	+4.4
	1.38	-12.7	1.45	+3.1
Mg^{++}	0.17	+13.3	0.114	+2.0
	0.40	0.0	0.300	-0.2
Na^{+}	0.13	+30.0	0.157	+0.4
	0.79	-12.2	0.500	-0.1
K^{+}	[0.033	-7.4]	0.033	-7.4
	[0.270	+0.5]	0.270	+0.5
NH_4^{+}	0.10	+5.3	0.30	+1.1
	0.92	-3.2	2.05	+0.1
$SO_4^{=}$	0.98	-2.0	5.12	+0.3
	7.87	-1.6	10.24	-0.2
NO_3^{-}	1.20	-2.4	0.49	+1.6
	3.80	+3.5	1.68	-0.5
Cl^{-}	0.17	-5.6	1.41	+4.6
	1.00	+0.3	2.81	+4.4

Table 2. Precision for detection limit, median concentration, and high concentration determined from event and weekly precipitation samples collected from April 1980-1981 for the Analytical Chemistry Laboratory (ANL samples) and the Central Analytical Laboratory (NADP samples). Values in brackets were assumed.

	ANL Analyses		NADP Analyses	
Parameter	Values	Precision, %	Values	Precision, %
Precipitation amount, g	2	±100.0	2	±100.0
	300	±1.9	300	±1.9
	1300	±0.5	1300	±0.5
Titration, μeq/L	2.5	±100.0	[2.5	±100.0]
	40	±2.3	[40	±2.3]
	132	±4.5	[132	±4.5]
pH	Not Applicable		Not Applicable	
	[3.06	±3.0]	3.06	±3.0
	[4.08	±10.1]	4.08	±10.1
Conductivity, μS/cm	Not Applicable		Not Applicable	
	[35.5	±9.7]	35.5	±9.7
	[401	±2.3]	401	±2.3
Ions, mg/L				
Ca^{++}	0.01	±100.0	0.02	±100.0
	0.32	±1.6	0.35	±4.0
	1.38	±6.8	1.45	±2.6
Mg^{++}	0.003	±100.0	0.002	±100.0
	0.17	0.0	0.114	±3.1
	0.40	0.0	0.300	±2.0
Na^{+}	0.02	±100.0	0.004	±100.0
	0.08	±4.2	0.157	±1.4
	0.450	±8.0	0.500	±1.5
K^{+}	0.05	±100.0	0.004	±100.0
	0.131	±38.6	0.033	±10.7
	0.39	±5.3	0.270	±3.1
NH_4^{+}	0.02	±100.0	0.02	±100.0
	0.10	±2.1	0.30	±10.1
	1.42	±3.5	2.05	±3.3
$SO_4^{=}$	0.05	±100.0	0.10	±100.0
	3.54	±4.6	5.12	±1.7
	6.07	±4.1	10.24	±1.2
NO_3^{-}	0.01	±100.0	0.02	±100.0
	1.47	±7.6	0.49	±5.1
	3.93	±5.0	1.68	±3.6
Cl^{-}	0.04	±100.0	0.05	±100.0
	0.106	±17.0	1.41	±1.4
	0.243	±8.7	2.81	±2.1

standard deviation of the baseline noise. The bias at the detection limit is assumed to be zero. Bias and precision for ANL precipitation chemistry data were determined from 6 analyses of prepared standards that approximated the median and high concentrations in the comparison study. ANL bias and precision for pH, conductivity, and potassium were not determined. Bias and precision for NADP samples were taken from data given by Stensland et al. (1980) for similarly appropriate concentrations. All ANL and NADP samples were titrated by this Section, and bias and precision were determined from the 1980 USGS chemistry round robin (e.g., Sisterson, 1981). Precipitation amounts were determined from weighing both NADP and ANL samples by this Section. Although NADP buckets were preweighed by the Central Analytical Laboratory, the NADP buckets were reweighed by this Section and the resulting values were taken to be the certified value. Bias and precision for NADP and ANL parameters compared in the weekly versus event study are shown in Tables 1 and 2, respectively.

The data suggest that accuracy is better at the Central Analytical Laboratory. However, the Analytical Chemistry Laboratory accuracy is based upon far fewer sample repetitions, which may result in the larger uncertainties.

Precision and bias as a function of concentration are being incorporated into computer programs that first correct individual ANL and NADP samples according to appropriate bias and then assign appropriate precision. When samples are summed, appropriate precipitation-weighted precision will be determined and compared to the differences in weighted-mean concentrations corrected for bias to determine the significance of the differences.

References

Sisterson, D. L., 1981: Results of the 1981 rain chemistry round robin, This report.

Sisterson, D. L. and D. Wagner, 1980: A comparison of the chemistry of event and weekly precipitation samples in northern Illinois -- A preliminary report, Part 2, Argonne National Laboratory Radiological and Environmental Research Division ANL-80-115, Part IV, pp. 72-74.

Sisterson, D. L. and B. Wurfel, 1980: A comparison of the acidity of event and weekly precipitation samples in northern Illinois -- A preliminary report, Part 1, Argonne National Laboratory Radiological and Environmental Research Division ANL-80-115, Part IV, pp. 68-71.

Sisterson, D. L. and B. Wurfel, 1981: Seasonal and annual comparison of weekly and event sampling of precipitation chemistry, This report.

Stensland, G., R. Semonin, M. Peden, V. Bowersox, F. McGurk, L. Skowron, M. Slater, and R. Stahlhut, 1980: NADP quality assurance report: Central Analytical Laboratory, 1-79 to 12-79, Illinois Institute of Natural Resources, State Water Survey Division, Champaign, IL 61820.

RESULTS OF THE 1981 RAIN CHEMISTRY ROUND ROBIN

D. L. Sisterson

In March 1981, 13 chemistry laboratories participated in a rain chemistry round robin sponsored by the U.S. Geological Survey (USGS). This was the second rain chemistry round robin (Sisterson, 1980) in which the Analytical Chemistry Laboratory (ACL) at Argonne participated since it began analyzing precipitation samples in 1979 for this Section's acid rain program. USGS provided four samples; the B and N samples were rain simulants representing when diluted typical high and low concentrations, respectively, of environmental pollutants found in rainwater samples. The AC and FL samples were natural rain samples representing high and low concentrations, respectively.

ACL analyzed for $SO_4^{=}$, NO_3^{-}, Cl^{-}, F^{-}, NH_4^{+}, K^{+}, and Na^{+} by liquid ion chromatography, and for Ca^{++} and Mg^{++} by flame atomic absorption. Conductivity and pH measurements were determined by cell methods and electrodes, respectively, by this Section. Only one analysis of each sample was performed. The methods of analysis and number of determinations by the other laboratories were not available.

Although the USGS provided the chemical data for the simulated precipitation reference materials (B and N), no certified values were given for the natural rain samples. Reference values for the rain samples were obtained by computing mean concentrations for each parameter from the values reported by the 13 participating laboratories. For comparison, the same was done for the simulated samples. An asterisk indicates ANL or USGS values that fell outside the 95% confidence level (2 standard errors) of the computed reference values. The results of the rain chemistry round robin for samples B, N, AC and FL are shown in Table 1-4, respectively.

For sample B, the ACL $[K^{+}]$ was low and $[NH_4^{+}]$ high (the brackets signify concentration), and $[Mg^{++}]$, $[K^{+}]$, and $[Na^{+}]$ were low for sample N. USGS reference conductivity and pH values were high for sample B, and $[Na^{+}]$ was low and pH value high for sample N. ACL $[NH_4^{+}]$ was high for sample AC and $[K^{+}]$ was low for sample FL.

Table 1. Results of the USGS precipitation chemistry round robin for sample B. S.E. is the standard error. All values are in mg/L except conductivity (μS/cm) and pH. Difference is individual-laboratory mean.

Parameter	Number of values	All lab mean	2 x S.E.	USGS	Difference	ANL	Difference
Ca^{++}	11	0.65	±0.05	0.65	0.00	0.63	-0.02
Mg^{++}	11	0.27	±0.05	0.23	-0.04	0.24	-0.03
K^{+}	10	0.55	±0.05	0.51	-0.04	0.45*	-0.10
Na^{+}	11	0.59	±0.08	0.56	-0.03	0.57	-0.02
NH_4^{+}	10	0.63	±0.08	0.66	+0.03	0.79*	+0.16
Cl^{-}	11	3.19	±0.15	3.27	+0.08	3.24	+0.05
NO_3^{-}	11	1.80	±0.40	2.15	+0.35	2.08	+0.28
SO_4	11	2.38	±0.48	2.35	-0.03	1.96	-0.42
Conductivity	10	40.65	±2.10	43.50*	+2.85	42.11	+1.46
pH	10	4.21	±0.08	4.35*	+0.14	4.20	-0.01

Table 2. Same as Table 1 except sample is N.

Parameter	Number of values	All lab mean	2 x S.E.	USGS	Difference	ANL	Difference
Ca^{++}	11	0.25	±0.04	0.25	0.00	0.22	-0.03
Mg^{++}	11	0.08	±0.02	0.06	-0.02	0.05*	-0.03
K^{+}	10	0.20	±0.07	0.16	-0.04	0.11*	-0.09
Na^{+}	11	0.33	±0.04	0.28*	-0.05	0.26*	-0.07
NH_4^{+}	10	0.20	±0.03	0.21	+0.01	0.20	0.00
Cl^{-}	11	0.89	±0.12	0.91	+0.02	0.86	-0.03
NO_3^{-}	11	0.73	±0.13	0.83	+0.10	0.65	-0.08
SO_4	11	0.83	±0.27	0.78	-0.05	0.57	-0.26
Conductivity	10	12.61	±1.52	13.20	+0.59	12.14	-0.47
pH	10	4.83	±0.11	5.03*	+0.20	4.83	0.00

Table 3. Same as Table 1 except sample in AC.

Parameter	Number of values	All lab mean	2 x S.E.	ANL	Difference
Ca^{++}	11	1.48	±0.07	1.44	-0.04
Mg^{++}	11	0.31	±0.02	0.30	-0.01
K^{+}	10	1.15	±0.08	1.08	-0.07
Na^{+}	11	1.73	±0.15	1.66	-0.07
NH_4^{+}	10	0.68	±0.09	0.83*	+0.15
Cl^{-}	11	2.40	±0.24	2.53	+0.13
NO_3^{-}	11	2.77	±0.63	3.23	+0.46
SO_4	11	1.52	±0.37	1.14	-0.38
conductivity	10	26.19	±0.53	28.56	+2.37
pH	10	6.25	±0.16	6.36	+0.11

*Values that fell outside the 95% confidence level (2 standard deviations).

Table 4. Same as Table 1 except sample is FL.

Parameter	Number of values	All lab mean	2 x S.E.	ANL	Difference
Ca^{++}	11	1.11	±0.13	1.17	+0.06
Mg^{++}	11	0.20	±0.03	0.20	0.00
K^{+}	10	0.32	±0.04	0.26*	-0.06
Na^{+}	11	1.40	±0.06	1.36	-0.04
NH_4^{+}	10	0.04	±0.02	0.05	+0.01
Cl^{-}	11	1.90	±0.06	1.84	-0.06
NO_3^{-}	11	1.23	±0.27	1.37	+0.14
SO_4	11	0.61	±0.28	0.38	-0.23
Conductivity	10	16.86	±0.99	16.35	-0.51
pH	10	6.22	±0.14	6.28	+0.06

Table 5. Comparison of chemical simulant and natural rain sample variances for appropriate concentration.

Parameter	Simulant Sample	Simulant all lab mean	Simulant σ	Natural Rain Sample	Natural Rain all lab mean	Natural Rain σ
Ca^{++}	B	0.65	±0.09	FL	1.11	±0.21
Mg^{++}	B	0.27	±0.09	AC	0.31	±0.04
K^{+}	B	0.55	±0.09	FL	0.32	±0.06
Na^{+}	B	0.59	±0.14	FL	1.40	±0.10
NH_4^{+}	B	0.63	±0.13	AC	0.68	±0.14
Cl^{-}	B	3.19	±0.25	AC	2.40	±0.39
NO_3^{-}	B	1.80	±0.66	FL	1.23	±0.44
SO_4	N	0.83	±0.45	FL	0.61	±0.46
conductivity	N	12.61	±0.76	FL	16.86	±1.56

ACL $[K^{+}]$ values are significantly lower in 3 of the 4 samples. Liquid ion chromatography is typically less sensitive to K^{+} than other analytical methods (Williams, 1981). Also, $[NH_4^{+}]$ were significantly higher in only the high concentration samples. The higher the combined concentrations of K^{+} and NH_4^{+} in a single sample, the less the resolution of each ion (Williams, 1981). The $[Na^{+}]$ and $[Mg^{++}]$ differences in sample N are attributed to accuracy errors that may result from single determinations of ions at low concentrations.

*Values that fell outside the 95% confidence level (2 standard deviations).

This rain chemistry round robin included natural rain samples. Typically, rain samples are difficult to use as reference samples because of poor ion stability (e.g., Peden and Skowron, 1978). Nevertheless, as shown in Table 5, the standard deviations for simulant and natural rain samples are quite similar for these approximately equal mean concentrations determined from the 13-laboratory average.

References

Peden, M. E. and L. M. Skowron, 1978: Ionic stability of precipitation samples, Atmos. Environ. 12, 2343-2349.

Sisterson, D. L., 1980: Results of the 1980 rain chemistry round robin, Argonne National Laboratory Radiological and Environmental Research Division Annual Report, ANL-80-115 Part IV, pp. 65 67.

Williams, F., 1981: Personal communication, Analytical Chemistry Laboratory, Chemical Engineering Division, Argonne National Laboratory.

ERRORS IN pH ELECTRODE MEASUREMENT

D. L. Sisterson and B. Wurfel

The current interest in acid precipitation has placed great demands on the ability to measure accurately the pH of solutions having low ionic strength. With conventional electrodes, errors in pH measurements and acidity determinations can arise from streaming and liquid-junction potentials (e.g., Feldman, 1956). Furthermore, electrodes do not measure hydrogen ion concentration (i.e., acidity) directly, but rather hydrogen ion activity. Conversion from activity to concentration depends upon ionic strength of the sample and can become complicated. Analysis of errors common to pH electrodes are therefore desired so that the reliability of pH measurements can be determined.

The Debye-Huckel expression (Strumm and Morgan, 1970) is appropriate for conversion from H^+ activity to H^+ concentration for the typical range of ionic strengths of precipitation. Omission of this conversion results in an error of -0.01 ± 0.01 pH units (Sisterson and Wurfel, 1982). This error was determined by considering precipitation samples with extremely high and low ionic strengths chosen from the National Atmospheric Deposition Program network. Here, and throughout the text, the uncertainty given is ± 2 standard deviations.

Electrodes and pH meters approximate the pH of a solution by utilizing the Nernst equation, which relates the potential measured by the electrode in a standard buffer solution to that in the precipitation sample. Flow of the reference electrolyte solution through the ceramic junction causes an erroneous liquid-junction potential (e.g. Sisterson and Irving, 1979), which is a function of the ionic strength of the solution. When the ionic strengths of the buffer and the sample are dissimilar, differences between junction potentials can lead to errors as large as ± 0.02 pH units (Eisenman, 1967).

Stirring the precipitation sample during pH measurement assures uniform concentration of the sample and fast pH electrode response. However, stirring also produces a streaming potential that can seriously affect the pH measurement. A comparison of stirred and unstirred pH measurements has been

made for 67 precipitation samples collected at Argonne. The mean difference was -0.04 ± 0.10 pH units. A stirring rate of 2 ± 1 revolutions per second (used in the study) probably produces the large departures from the mean difference. At faster rates, the pH differences become quite large; Galloway et al. (1979) report observations indicating pH differences greater than 0.50 pH units due to streaming potential. To eliminate this error, the precipitation sample can be thoroughly agitated and allowed to come to rest before taking a pH reading. Table 1 summarizes the errors associated with a properly operating pH electrode. While the individual errors are small, the causes of error are independent and thus the variances are additive. The total error (at rest after stirring) appears quite small; yet, there are still other sources of uncertainty (not listed here) in electrode performance that could significantly affect the measured pH (Bigalow, 1982).

Table 1. Summary of individual pH errors for a properly functioning electrode.

Error type	Bias	2σ
No Debye-Huckel correction	-0.01	±0.01
Liquid-junction potential	0.00	±0.02
Streaming potential (2 ± 1 revolutions per second at Argonne)	-0.04	±0.10
Total error (at rest after stirring)	-0.01	±0.02
Total error (stirred)	-0.05	±0.10

To increase confidence in absolute pH measurements, the acidity of precipitation can be determinated from simple titration. Gran (1950, 1952) developed a procedure for the analysis of titration data that allows the determination of the hydrogen ion concentration directly. Gran's function uses only the differences in measured pH; therefore, streaming and liquid junction potentials, and conversion of activity to concentration are eliminated as long as the temperature and the stirring rate during titration are constant. Typical titration errors were determined to be -0.01 ± 0.03 pH units; however, for Argonne non-constant stirring rates, titration errors were estimated to be -0.01 ± 0.08 pH units, (Sisterson and Wurfel, 1982). The observed difference between hydrogen ion activity determinations by pH electrode and hydrogen ion concentration determinations by titration for 48

samples collected at Argonne was -0.03 ± 0.10 pH units. The agreement between estimated and observed errors appears reasonable with most of the error due to stirring rate inconsistencies. Table 2 summarizes these errors.

The uncertainty in pH electrode measurements for individual precipitation samples is relatively large. This study indicates that subtle differences in precipitation acidity are difficult to determine accurately. To reduce this uncertainty in determining trends involving small pH differences, many samples must be collected.

Table 2. Summary of the errors associated with electrode and titration determination of acidity.

Total estimated error	Bias	2σ
Constant stirring	-0.01	±0.03
Non-constant stirring	-0.01	±0.08
Observed error		
Non-constant stirring	-0.03	±0.10

References

Bigalow, D., 1982: National Atmospheric Deposition Program Instruction Manual -- Site Operation, National Resource Ecology Laboratory, Colorado State University, Fort Collins, CO 80523.

Eisenman, G., 1967: Glass electrodes for hydrogen and other cations. Marcel Dekker, Inc, New York.

Feldman, I., 1956: Use and abuse of pH measurements, Analy. Chem. 28, 1859-1855.

Galloway, J. N., B. J. Cosby, Jr., and G. E. Likens, 1979: Acid precipitation: Measurement of pH and acidity, Limnol. Oceanogr. 24, 1161-1165.

Gran, G., 1950: Determination of the equivalent point in potentiometric titrations, Acta Chem. Scandi. 4, 559-577.

Gran, G., 1952: Determination of the equivalence point in potentiometric titrations, Part II, Analyst 77, 661-671.

Strumm, W. and J. Morgan, 1970: Aquatic Chemistry, Wiley-Interscience, New York.

Sisterson, D. L., and P. M. Irving, 1979: pH measurements of rain, Argonne National Laboratory Radiological and Environmental Research Division Annual Report ANL-79-65, Part IV, pp. 61-64.

Sisterson, D. L., and B. E. Wurfel, 1982: Use of pH electrodes and titration methods to estimate acidity of precipitation samples, Bull. Am. Meteorol. Soc., submitted.

EFFECTS OF CHICAGO EMISSIONS ON LOCAL PRECIPITATION CHEMISTRY--A PRELIMINARY REPORT

D. L. Sisterson

This Section began collecting event precipitation samples at the Jardine Water Purification Plant on Chicago's lakefront, just east of the downtown area, in June 1981. These samples are being compared with corresponding event samples collected at Argonne, ~ 40 km SW of the water plant, to determine the effect on local precipitation chemistry of pollutant emissions in greater Chicago. The collection procedures are discussed elsewhere (Sisterson and Wurfel, 1980). The collection site is free of nearby tall buildings, and the local air quality is not dominated by any single source (Illinois EPA, 1979). The Jardine collector is placed near the west edge of the roof of the administration building (~ 21 m above the lake level and ~ 200 m from the lakeshore) to reduce the chance of lake spray contamination.

Stratification of the Argonne (ANL) and Chicago (CHI) sample pairs according to wind direction aids in evaluation of the urban influence on local precipitation chemistry. Variation in precipitation intensity and rainfall amount between the two sites can be expected to affect significantly single event sampling, particularly in the case of convective storms. Total precipitation amounts are expected to be similar, however, when summed over sufficiently long time periods. This study is expected to continue for one year.

To minimize potential meteorological variability, total wet deposition (concentration times rain amount) comparisons should be used for samples collected from convective storms as long as there is no significant difference in rain amount. All events collected in this preliminary study were convective; hence, data are presented in terms of wet deposition (μeq). Precipitation samples were analyzed by the Analytical Chemistry Laboratory at Argonne. Storm intensity and wind direction information were determined from observations and daily surface weather maps, respectively.

From June through November, 30 pairs of event samples were collected and stratified according to upwind quadrants, based upon surface wind

direction prior to the onset of precipitation. Large differences occurred between ANL and CHI rain amounts for SW, SE, and NW wind direction quadrants. In an attempt to reduce the meteorological variability due to these differences, the ANL and CHI total wet deposition values for each chemical species were normalized by the respective precipitation amount for that quadrant. Air quality data from modified Lundgren impactors (Cunningham et al., 1974) at the two sites will be used in addition to the precipitation chemistry data for $SO_4^=$, NO_3^-, and NH_4^+ to estimate the affect of storm intensity and rain rate on precipitation chemistry. Table 1 shows those normalized ANL and CHI wet deposition values for each quadrant. The differences between ANL and CHI normalized total wet deposition values are shown in Table 2.

Normalized total wet deposition values (weighted average concentrations) shown in Table 1 are greatest at both sites for nearly all chemical species when winds are from the SE quandrant. This is not surprising since most of the refinery and industrial complexes within 150 km are located SE of the urban area. Also, long-range transport from the Ohio River valley is most likely with SE winds. Lowest values for both ANL and CHI samples generally occur when winds are from the NW, a direction free from large industrial sources.

While actual differences between ANL and CHI chemical species (Table 2) may not accurately quantify Chicago's influence on precipitation chemistry, trends in those differences may, in most cases, be representative of the urban influence. Generally, CHI samples have higher normalized total wet deposition values for each chemical species for all wind directions with the following exceptions. ANL samples are more acidic than CHI samples in all seasons (field determinations), have more deposition of NH_4^+ for SW winds and more NO_3^- and $SO_4^=$ for NW winds. Usually, the more intense the rain rate, the less the pollutant concentration in precipitation because of dilution. This may explain the reversal of the trend in NO_3^- and $SO_4^=$ values for NW winds (CHI received 91.49% more precipitation). Increased urban NH_4^+ may be primarily responsible for the mitigation of CHI precipitation acidity.

It is surprising that CHI samples have higher normalized wet deposition values for NE winds when Argonne is directly downwind of the city. Since the rain amounts with the NE wind are similar, meteorological

Table 1. Normalized total wet deposition values for chemical species analyzed in Argonne (ANL) and Chicago (CHI) rain samples stratified by wind quadrants. The number of events collected for each quadrant are given in parenthesis. All values are μeq/L except where indicated.

Quadrant	H^+ (field pH) ANL	H^+ (field pH) CHI	H^+ (lab pH) ANL	H^+ (lab pH) CHI	Conductivity, μS/cm/L ANL	Conductivity, μS/cm/L CHI	Rain, g x 10^3 ANL	Rain, g x 10^3 CHI
SW (8)	88.67	67.54	49.66	65.64	27.00	33.70	8.57	13.88
SE (10)	81.58	72.17	97.39	88.12	40.89	40.59	14.43	8.26
NW (7)	49.13	21.88	51.15	22.17	27.81	19.01	2.87	7.71
NE (5)	53.52	45.02	48.50	46.56	22.13	21.97	7.27	7.47
	Ca^{++}		Mg^{++}		K^+		Na^{++}	
SW (8)	11.46	14.96	2.65	3.35	0.23	0.09	1.30	0.53
SE (10)	9.35	13.98	2.67	4.19	0.04	0.07	0.37	0.92
NW (7)	8.36	8.61	2.20	3.31	0.00	0.00	0.11	0.10
NE (5)	7.47	7.94	2.00	2.16	0.99	0.58	1.72	1.71
	NH_4^+		NO_3^-		Cl^-		$SO_4^=$	
SW (8)	31.55	30.03	22.29	26.90	0.35	2.45	63.72	72.63
SE (10)	28.23	38.48	30.45	33.45	2.67	3.38	92.54	95.39
NW (7)	23.45	33.24	23.10	15.94	1.92	0.90	53.62	53.22
NE (5)	12.94	19.67	20.69	26.88	0.69	1.54	49.40	55.78

Table 2. Percent difference [(CHI-ANL)/mean] x 100% between Argonne (ANL) and Chicago (CHI) normalized total wet deposition values shown in Table 1 according to wind quandrant.

Quadrant	H^+ (pH field)	H^+(pH lab)	Conductivity	Rain
SW (8)	-27.05	+27.72	+22.08	+47.31
SE (10)	-12.24	-9.99	-0.74	-54.39
NW (7)	-76.75	-79.05	-37.59	+91.49
NE (5)	-17.25	4.08	-0.73	+2.70
	Ca^{++}	Mg^{++}	K^+	Na^+
SW (8)	+26.50	+23.33	-87.50	-84.15
SE (10)	+39.69	+44.31	+54.55	+85.27
NW (7)	+2.95	+40.29	0.00	-9.52
NE (5)	+6.10	+7.69	-52.23	-0.58
	NH_4^+	NO_3^-	Cl^-	$SO_4^=$
SW (8)	-4.94	+18.74	+150.00	+13.07
SE (10)	+30.73	+9.39	+23.47	+3.03
NW (7)	+34.54	-36.68	-72.34	-0.75
NE (5)	+41.28	+26.02	+76.23	+12.13

variability (storm intensity, rain rate) is minimal. Most NE quadrant samples, however, had been collected from shallow convective storms of relatively long duration. Typically, wind speed had been lighter and more variable for this wind direction during precipitation. Complicated flow patterns would therefore make source/receptor relationships unclear.

Precipitation acidity is highest with the SE and SW winds cases. However, seasonal variation has not been taken into account and may also play an important role in acidity variation (Sisterson and Wurfel, 1981). With additional samples and completion of the air quality data analysis, more information will be gained about Chicago's effect on local precipitation chemistry.

References

Cunningham, P. T., S. A. Johnson, and R. Ty. Yang, 1974: Variation in chemistry of airborne particulate material with particle size and time, Atmos. Environ. 8, 131-135.

Illionis EPA, 1979: Technical analysis of the state implementation plan for the attainment and maintenance of the suspended particulate ambient air quality standards in the Chicago air quality maintenance area. Division of Air Pollution Control, Illinois Environmental Protection Agency, 2200 Churchill Road, Springfield, IL, 62706.

Sisterson and Wurfel, 1980: A comparison of the acidity of event and weekly precipitation samples in northern Illinois--A preliminary report, Part I, Argonne National Laboratory Radiological and Environmental Research Division Annual Report ANL-80-115, Part IV, pp. 68-71.

Sisterson and Wurfel, 1981: Seasonal and annual comparison of weekly and event precipitation chemistry, this report.

PUBLICATIONS BY THE STAFF OF THE ATMOSPHERIC PHYSICS SECTION FOR THE PERIOD JANUARY-DECEMBER 1981

Journal Articles, Book Chapters, Etc.

J. D. Shannon
A MODEL OF REGIONAL LONG-TERM AVERAGE SURFACE ATMOSPHERIC POLLUTION, SURFACE REMOVAL, AND NET HORIZONTAL FLUX
Atmos. Environ. 15(5), 689-701.

C. M. Sheih
PASQUILL-TAYLOR DISPERSION PARAMETERS OVER WATER NEAR SHORE
Atmos. Environ. 15(1), 101-105.

M. L. Wesely, D. R. Cook, and R. M. Williams
FIELD MEASUREMENTS OF SMALL OZONE FLUXES TO SNOW, WET BARE SOIL, AND LAKE WATER
Boundary-Layer Meteorol. 20(4), 459-571.

B. B. Hicks, G. D. Hess, M. L. Wesely, T. Yamada, P. Frenzen, R. L. Hart, D. L. Sisterson, P. E. Hess, F. C. Kulhanek, R. C. Lipschutz, and G. A. Zerbe
THE SANGAMON FIELD EXPERIMENTS: OBSERVATIONS OF THE DIURNAL EVOLUTION OF THE PLANETARY BOUNDARY LAYER OVER LAND
Argonne National Laboratory Radiological and Environmental Research Division Topical Report ANL/RER-81-1, 173 pp.

B. B. Hicks and M. L. Wesely
HEAT AND MOMENTUM TRANSFER CHARACTERISTICS OF ADJACENT FIELDS OF SOYBEANS AND MAIZE
Boundary-Layer Meteorol. 20, 175-195.

B. B. Hicks
AN EXAMINATION OF TURBULENCE STATISTICS IN THE SURFACE BOUNDARY LAYER
Boundary-Layer Meteorol., 21, 389-402.

G. D. Hess, B. B. Hicks, and T. Yamada
THE IMPACT OF THE WANGARA EXPERIMENT
Boundary-Layer Meteorol. 20, 135-174.

T. Yamada
A NUMERICAL SIMULATION OF NOCTURNAL DRAINAGE FLOW
J. Meteorol. Soc. of Japan, 59, 108-122.

Conference Papers and Abstracts

Bruce B. Hicks, M. L. Wesely, and Jack L. Durham
CRITIQUE OF METHODS TO MEASURE DRY DEPOSITION
Proceedings of the Energy and Environmental Chemistry, Volume Two, Acid Rain, National ACS Meeting, Atlanta, GA, pp. 205-223, 1 April 1981.

T. Yamada
A NUMERICAL SIMULATION OF FOREST CANOPY FLOW
Proceedings of the 2nd Conf. on Mountain Meteorology, Nov. 9-12, 1981, AMS, Steamboat Springs, CO, 4.1, pp. 88-90.

Bruce B. Hicks
WET AND DRY SURFACE DEPOSITION OF AIR, POLLUTANTS, AND THEIR MODELING
Proceedings of the Conservation of Historic Stone Buildings and Momuments, Washington, DC, 2-4 Feb. 1981 (National Academy of Sciences).

R. L. Coulter
NOCTURNAL WIND PROFILE CHARACTERISTICS
Proceedings of the International Symposium on Acoustic Remote Sensing of the Atmosphere and Oceans, The University of Calgary, Calgary, Alberta, Canada, June 22-25, 1981, (Abstract), pp. VI-I - VI-II.

T. J. Martin
ACOUSTIC SOUNDER INTENSITY DISPLAY TECHNIQUES
Proceedings of the International Symposium on Acoustic Remote Sensing of the Atmosphere and Oceans, The University of Calgary, Calgary, Alberta, Canada, June 1981, pp. II-26 - II-29.

M. L. Wesely
ON THE EXCHANGE OF TRACE MATERIALS ACROSS INTERFACIAL SUBLAYERS
IAMAP Symposium on the Role of Oceans in Atmospheric, 17-29 August 1981, Hamburg, F. R. Germany, (Abstract), p. 74 of ICACGP.

C. M. Sheih
A REPLY TO GIFFORD COMMENTS ON "ON LATERAL DISPERSION COEFFICIENTS AS A FUNCTION OF AVERAGING TIME"
J. Appl. Meteorol. 20, 213-214 (February 1981).

C. M. Sheih
A REPLY TO ROWE COMMENTS ON "ON LATERAL DISPERSION COEFFICIENTS AS A FUNCTION OF AVERAGING TIME"
J. Appl. Meteorol. 20, 730 (June 1981).

C. M. Sheih and W. Heilman
PRELIMINARY INVESTIGATIONS OF POLLUTANT DISTRIBUTION IN A TWO-DIMENSIONAL STREET CANYON
Preprint of the Fifth Symposium on Turbulence, Diffusion, and Air Pollution, AMS, 9-13 March 1981, Atlanta, GA, pp. 192-193.

J. D. Shannon
OPTIMAL SPATIAL DESIGN FOR AUGMENTATION OF A NETWORK OF RECEPTORS FOR WET DEPOSITION OF SULFUR
Preprint of the Fifth Symposium on Turbulence, Diffusion, and Air Pollution, AMS, 9-13 March 1981, Atlanta, GA, pp. 136-137.

I.-Y. Lee
SIMULATION OF OZONE IN THE PLANETARY BOUNDARY LAYER
Preprint of the Fifth Symposium on Turbulence, Diffusion, and Air Pollution, AMS, 9-13 March 1981, Atlanta, GA, pp. 92-93.

R. L. Coulter

CIRCULATION CHRACTERISTICS DURING ASCOT 1980

Preprint of the 2nd Conference on Mountain Meteorology, 9-12 November 1981, Steamboat Springs, CO, (AMS), pp. 316-320.